PARALLEL SESSION ON ELECTROMAGNETIC INTERACTIONS OF HADRONS

ELASTIC AND INELASTIC ELECTRON SCATTERING FROM THE DEUTERON AT LARGE MOMENTUM TRANSFER

B.T.Chertok
American University, Washington, D.C., USA

The deuteron form factor $F_D(q^2)$ and inelastic structure function, $\nu W_{2D}(q^2,\nu)$, at threshold both provide excellent examples of the continuity between nuclear and particle physics at the microscopic level. The deuteron could be viewed as a very complex system at low and moderate q^2 ($\lesssim 1$ GeV^2). That is, this elementary two-body bound state at $q^2=0$ could become a complex system with increasing q^2 by the addition, for example, of isobar resonances ($\Delta\Delta$ and $N'N$) to the N-N ground state and with the increasing importance at the electromagnetic vertex of two-body meson-exchange currents.

However, the probing of the deuteron's electromagnetic structure at large q^2 ($\gtrsim 1$ GeV^2) appears to reveal a marvelous simplicity[1]. From a dimensional scaling quark model approach Brodsky had predicted that the deuteron form factor would diminish as $(q^2)^{-1}$ after the two-nucleon's structure was removed at reduced q^2[2], i.e.

$$F_D / F_p^2(q^2/4) \sim 1/q^2. \qquad (1)$$

This prediction has been confirmed in our experiment at SLAC[1] as seen in figs.1 and 2.

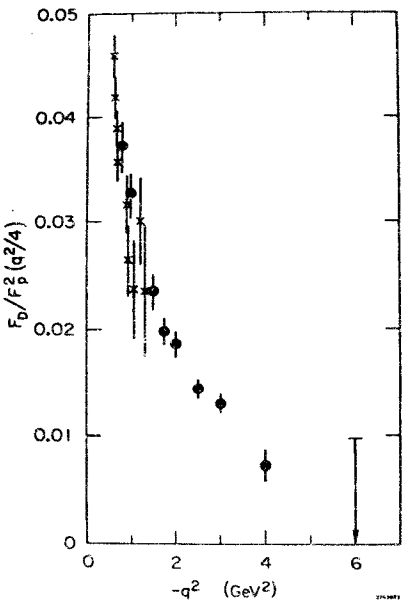

Fig.1

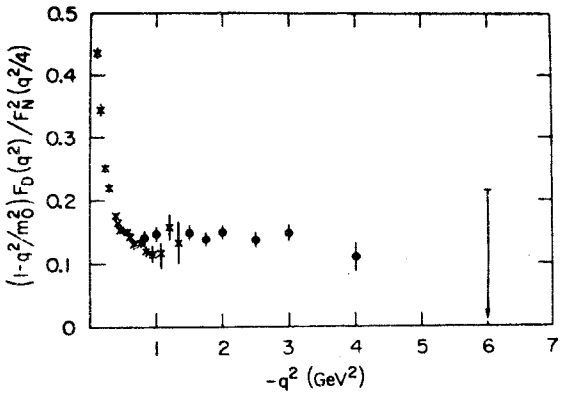

Fig.2

Thus, the underlying six-quark substructure of the deuteron is manifested in five powers of q^2; i.e., $F_p^2(\frac{q^2}{4})/q^2 \sim (q^2)^{-5}$ in agreement with quark counting, so that,

$$(q^2)^{n-1} F_n \longrightarrow \text{const}. \qquad (2)$$

This presentation will be divided into three sections:

1. The Asymptotic Elastic Form Factors of Hadrons and Nuclei, and the Continuity of Particle and Nuclear Dynamics;

2. Measurement of Inelastic e-D Scattering in the Threshold Region at large Momentum Transfer, and

3. Measurement of the Magnetic Form Factor of the Deuteron at $q^2=1$ GeV^2.

Professor Dally has presented our new measurement of the deuteron's magnetic form factor (section III) to this Conference.

I. The Asymptotic Elastic Form Factors

This study of the implications of the deuteron having an underlying six-quark substructure and the general connections between dimensional scaling and elastic form factors are summarized very briefly[3].

The large q^2 behaviour of the elastic form factor of a hadron or nucleus is related by dimensional counting to the number of its elementary constituents. Using the framework of a scale-invariant quark model, dimensional scaling

predictions are derived for the $B(q^2)/A(q^2)$ ratio in the Rosenbluth formula, multiple photon exchange corrections, and the mass parameters which control the onset of the asymptotic power law in the meson, nucleon, and deuteron form factors. A simple "democratic chain" model predicts that for large q^2, $F(q^2) \sim (1-q^2/m_n^2)^{1-n}$ where m_n^2 is proportional to the number of constituents n as in Fig.3a. Quark interchange of Fig.3b is used to calculate F_D with the results already presented in Fig.2. In the case

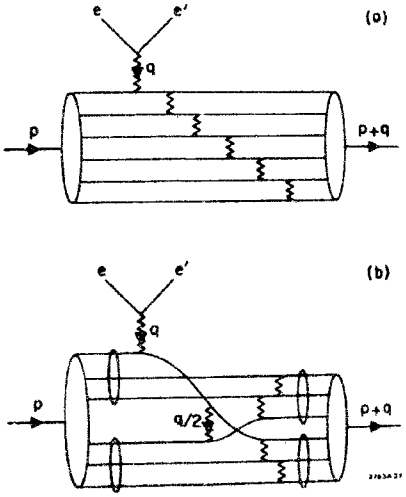

Fig.3

of nuclear targets (or systems with several scales of compositeness), we also define the "reduced" form factor $f_A(q^2) = F_A(q^2) / \prod_{a=1}^{A} F_a(q_a^2)$ in order to remove the minimal falloff of F_A due to the nucleon form factors at $q_a^2 = (m_a^2/M_A^2)q^2$. Dimensional counting predicts $(q^2)^{A-1} f_A(q^2) \to \text{const}$ as summarized in Table I.

TABLE I

Compositeness of Matter

Bound State	$F_i\left(\frac{m_i^2}{m_A^2} t\right)$	A	$f_A(t)$
e, μ, γ, q	1	1	t^0
π, K	1	2	t^{-1}
p, n	1	3	t^{-2}
D	$F_p(t/4)$	2	t^{-1}
^{3}He	$F_p(t/9)$	3	t^{-2}
^{4}He	$F_p(t/16)$	4	t^{-3}

A systematic comparison of the data for π, p, n, and deuteron form factors with the dimensional scaling quark model predictions are given. We also relate the deuteron form factor to (off-shell) fixed angle n-p scattering, and show that the experimental results for $t^5 F_D(t)$ are consistent with the magnitude of the s-wave function $u'(0)$ obtained from soft-core potentials. The relation of the dynamics of an underlying six-quark state of the deuteron to the nuclear potential and exchange current contributions is discussed. The scaling of $q^2 f_D(q^2)$ implies that the nuclear potential (after removing the effects of nucleon structure) displays the scale-invariant behaviour of a theory without a fundamental length scale. Predictions are also given for the structure functions, fragmentation, and large angle scattering of a nucleus.

II. Inelastic e-D Scattering at Threshold

At squared momentum transfers $0.8 \leq q^2 \leq 6.0$ $(\text{GeV/c})^2$, nine spectra of inelastic electron deuteron scattering were measured in the threshold region between 0 and 2.3% in $\Delta p/p$ below the elastic peak. The deuteron inelastic structure function νW_2 was extracted from these data. We found $\nu W_2(\omega')$ approaching a universal scaling curve and a close relation between νW_2 and the deuteron elastic structure function $A(q^2)$[4].

We report preliminary results of inelastic electron deuteron scattering in the threshold region at high momentum transfer q. The data were taken from a SLAC experiment[1] whose main purpose was to measure the elastic scattering cross sections and the deuteron structure function $A(q^2)$ at nine values of q^2 in the region $0.8 \leq q^2 \leq 6.0$ $(\text{GeV/c})^2$. The experimental conditions were such that we measured not only the elastic events, but also inelastic events from deuteron breakup and pion production between $0 \geq \Delta p/p_e \geq -2.3\%$, where p_e is the scattered electron momentum at the center of the elastic peak. The nine inelastic electron spectra span an unusual dynamic

region of large q^2 and small energy transfer $\nu = E_i - E_f$, the difference between initial and final electron energy. This region has not been explored before. Bjorken scaling is expected when both q^2 and ν are large compared with M_N^2, the square of the nucleon mass, as in deep inelastic electron scattering. The data presented here are on a scale where q^2 is expected to resolve the nucleons into fermion quark currents while ν is typical of excitation energies where nucleon-nucleon final state interaction effects may be significant.

We used the 20 GeV/c spectrometer of SLAC End Station A to detect scattered electrons at a fixed $\theta_e = 8^0$ from liquid deuterium, liquid hydrogen (for system calibration) and from a dummy target to determine the empty target background. To remove the elastic events out of the inelastic and background events, we used the 8 GeV/c spectrometer in coincidence with the 20 GeV/c spectrometer to detect the recoil deuterons with elastic kinematics.

Our results for the inelastic cross sections are the spectra of $d^2\sigma/d\Omega\, dE_f$ versus E_f. The error bars on the data points represent the statistical errors only. The systematical errors, mainly from uncertainties in $\Delta\Omega$ and the corrections, are estimated to $\pm 20\%$. The spectra rise almost exponentially with decreasing E_f, with a sharp rise from zero at the threshold.

For $q^2, \nu \to \infty$, it is observed that νW_2 becomes a function of the scaling variable ω' only, with $\omega' = 1 + W^2/q^2$ and $W^2 = M^2 + 2M\nu - q^2$, the square of the missing mass. Figure 4 shows a comparison of our data with data from Refs.5 and 7 on a νW_2 vs. ω' plot./6/. At q^2 below 2 $(GeV/c)^2$, we are not yet in the scaling region, but at $q^2 \geq 2$ $(GeV/c)^2$, our spectra merge with increasing q^2 into a universal $\nu W_2(\omega')$ curve. We find empirically that the spectra with $q^2 \geq 2$ $(GeV/c)^2$ can be described by the relation $\nu W_2 \sim (\omega' - 0.5)^n$, with $n = 6 \pm 0.5$. In an interesting paper presented to this Conference/8/,

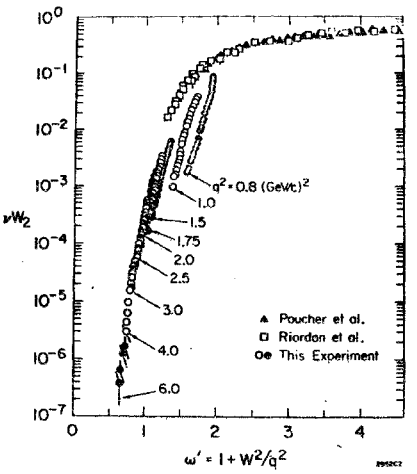

Fig. 4

Frankfurt and Strikman use a dispersion theory approach to the deuteron bound state and approximate their prediction for νW_{2D} as $.12\,(\omega' - \frac{1}{2})^{5.7}$ for $.55 \leq \omega' \leq 1$.

We find a close relation between the elastic $A(q^2)$ and W_2 at constant W^2. For W (Ref.6) close to M_d, we find empirically that our data follow the relation

$$W_2 \sim F_d^2(q^2) \cdot \varrho(W^2) \qquad (3)$$

with F_d given in Fig.5 and a function ϱ only depending on W^2 (see Fig.5).

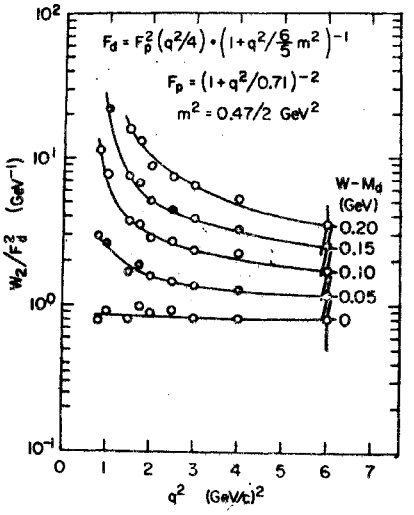

Fig.5

A connection between F and νW_2 near threshold has been given by Drell-Yan/9/ and West/10/ for the case of the proton:

$$\nu W_2 \sim x \cdot (1-x)^p, \quad F \sim (1/q^2)^{(p+1)/2}, \quad x = \frac{q^2}{2M\nu} \qquad (4)$$

If we extend this prediction to the deuteron, we postulate $p=9$, since $F\sim(1/q^2)^{-5}$. From our data, we could not get a reasonable fit within $4\leq p\leq 11$. So, we do not have any evidence that this connection works for the deuteron. However, we seem to be at too small q^2, ν -values to observe scaling in X .

If $G(q^2)$ is the excitation form factor of a resonance at $M=M_R$,

$$\nu W_2 = (M_R^2 - M_d^2 + q^2)\cdot[G(q^2)]^2\cdot\delta(W^2-M_R^2) \quad (5)$$

is its contribution to νW_2 in the narrow resonance approximation. This has been shown by Bloom and Gilman[11]. Our data indicate that this relation works in our case ($M_R\approx M_d$); i.e., $\nu W_2\sim q^2\cdot F_d^2\cdot\rho(W^2)$, similar to eqn. (3). Thus, our measurements indicate that νW_2 at threshold behaves like a resonance with $G(q^2)\sim F_d(q^2)$. This leads, in the language of the quark model, to be conclusion that, like in the elastic case, all six quarks participate in the threshold inelastic scattering process.

III. Measurement of Magnetic Structure Function of the Deuteron

At a momentum transfer squared of 1.0 $(GeV/c)^2$ the elastic scattering of electrons on deuterons has been measured at electron scattering angles of 8°, 60° and 82°. From these data we have extracted a value of $B(q^2)=1.55\pm.10\times10^{-5}$ for the deuteron. This measurement extends the range in momentum transfer by almost a factor of two over the previous measurements[12].

Large angle elastic eD scattering permits testing the dynamics of the deuteron's magnetic dipole moment, and large q^2 probes the short distance structure of these nuclear electromagnetic currents. Previous measurements of the deuteron's magnetic structure function $B(q^2)$ in the interval $0\leq q^2\leq 14\ F^{-2}$ (0.55 GeV^2) appear to be fully consistent with calculations using the impulse approximation[13]. These calculations use standard deuteron wave functions from N-N phenomenology and the measured nucleon form factors to compute $B(q^2)$. This approach appears to describe adequately any interaction effects in the deuteron at larger q^2 but leaves unexplained a discrepancy of 1-2% for the static magnetic dipole moment.

Our $A(q^2)$ is measured by scattering electrons at 8°, detecting the electron in the SLAC 20-GeV/c spectrometer and detecting, in coincidence with the electron, the deuteron in the SLAC 8-GeV/c spectrometer. The large angle data were taken at 60° and 82° where the electron was detected in the SLAC 1.6-GeV/c spectrometer, and the deuteron was detected as before. In order to calibrate the double-arm acceptances of these spectrometers, we also measured electron-proton scattering under the same conditions as those of the deuteron.

While it is not possible to rule out small contributions from exchange currents, our measurements are entirely consistent with the impulse approximation using empirical fits to the nucleon form factors. Thus, our measurement reaffirms the earlier observation made in Ref.[13] at lower q^2 to the same effect. Moreover, the impulse approximation for $B(q^2)$ is semsitive to the values for the nucleon form factors; in particular, the IJL form factors[14] yield a value of B which is 40% lower at $q^2=30\ f^{-2}$ than that using best fit to the data for G_{Mn}. We have also examined the effect of using different potential models for the deuteron with varying amounts of "D" state and find that the value of B is sensitive to these. For example, the Hamada-Johnson model with our most realistic nucleon form factors and a 7%D state wave function are estimated to produce a value of B approximately 30% higher at $q^2=1.0\ GeV/c^2$ than the Reid soft-core model we have used for our calculations. These uncertainties lead to considerable ambiguity in ascertaining the contribution - if any - of meson exchange currects in the magnetic structure of the deuteron.

Summary

Measurements of eD scattering at large values of q^2 as presented and discussed here, should enrich both nuclear and particle physics. In particular, the data[1,4,12] should provide important guidence for connecting the two fields of physics at the microscopic level. The constraints of quark-fermion currents and normal hadronic states must be simultaneously imposed and consistently satisfied. Measurement of elastic electromagnetic form factors to even larger q^2 will continue to play a unique role in physics.

References

1. R.Arnold, B.Chertok, E.Dally, A.Grigorian, C.Jordan, W.Schütz, R.Zdarko, F.Martin, B.Mecking. Phys.Rev.Lett., 35, 776 (1975); SLAC-PUB, 1596.
2. S.Brodsky. In "Proc. Int. Conf. on Few Body Problems in Nuclear and Particle Physics", edited by R.Slobodrian, B.Cujec, R.Ramavataram, p. 676, Les Presse de l'Univ. Laval, Quebec (1975), SLAC-PUB, 1497.
3. S.Brodsky, B.Chertok. SLAC-PUB. 1757 and 1759, submitted for publication.
4. W.Schütz and Collaboration of ref.1,submitted for publication.
5. J.S.Poucher et al. Phys.Rev.Lett., 32, 118 (1974).
6. For comparison with refs. 5 and 7, we calculated W^2 with M_N=.938 GeV. Our data are then in the range $-2.12 \leq W^2 \leq 0.76$ GeV^2. For comparison of νW_2 with F_d we defined W^2 with M_d = = 1.876 GeV ($3.52 \leq W^2 \leq 5.02$ GeV^2).
7. E.M.Riordan. Thesis, MIT Report No. COO-3069-176.
8. L.Frankfurt,M.Strikman.This Conference,265/B2
9. S.D.Drell, T.M.Yan. Phys.Rev.Lett., 24, 181 (1970).
10. G.B.West. Phys.Rev.Letters 24, 1206 (1970).
11. E.D.Bloom and F.J.Gilman. Phys.Rev.Letters 25, 1140 (1970).
12. F.Martin and collaboration of ref. 1, submitted for publication.
13. R.Rand et al., Phys.Rev., D8, 3229 (1973).
14. F.Iachello, A.Jackson and A.Lande.Phys.Lett., 43B, 191 (1973).

THE MEASUREMENT OF THE NUCLEON AND PION FORM FACTORS IN THE REGION OF TIME-LIKE 4-MOMENTUM TRANSFERS FROM 1.5 F^{-2} TO 3.0 F^{-2}

S.F.Berezhnev, T.D.Blokhintseva, A.V.Demyanov, A.V.Kuptsov, V.P.Kurochkin, L.L.Nemenov, G.I.Smirnov, D.M.Khazins

Joint Institute for Nuclear Research, Dubna

The experimental investigations[1-3] of the reaction of inverse electroproduction of pions (IEP)

$$\pi^- + p \to e^+ + e^- + n \qquad (1)$$

have been made at the pion energy of 275 MeV. The study [4] of reaction (1) was continued by means of a new experimental device, that permitted to detect 1043±46 events. The cross section of that part of the reaction which is determined by the geometry of the experimental device with the additional restriction $E_1, E_2 > 50$ MeV ($E_{1,2}$ is electron energy) is

$$\Delta\sigma = (4.80 \pm 0.43).10^{-33} \text{ cm}^2.$$

All events were separated into 5 groups according to the kinematic variable K^2, the average values of K^2 in each interval is 0.058, 0.0.73, 0.088, 0.103 and 0.119 (GeV/c)^2. The distributions of events as the function of $\cos\theta^*_{\pi N}$ between the pion and photon momenta (c.m.s.) were plotted for each group.

To analyse the experimental data the dispersion[6] model has been used. The formfactors $F_1^V(K^2)$ and $F_\pi(K^2)$ were taken as varying parameters upon which the differential cross sections are greatly dependent. The remaining form factors F_1^S, F_2^S, F_2^V and G_M^* affecting weakly the differential cross sections were calculated by means of the dipole formula. All the parameters were considered real. When determining the formfactors $F_1^V(K^2)$ and $F_\pi(K^2)$ the experimental cross sections $d\sigma/d\cos\theta^*_{\pi N}$ were fitted by theoretical ones calculated under the assumption that the formfactors should be equal.

Calculations performed by using the dispersion model describe very well all the experimental data. The results of determining the form

factor $F_1^V(K^2)$ and $F_\pi(K^2)$ under the condition of their equality are presented in Table 1.

Table 1

$K^2\left(\frac{GeV}{c}\right)^2$	0.058	0.073	0.088	0.103	0.119
Dispersion Model	$0.90\pm\pm0.07$	$1.00\pm\pm0.05$	$1.06\pm\pm0.05$	1.12 ± 0.05	$1.26\pm\pm0.04$

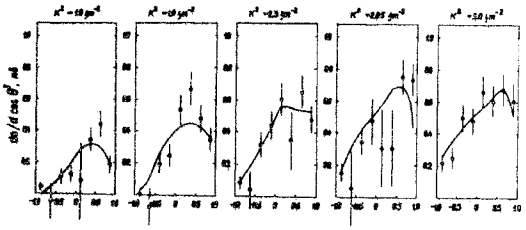

Fig.1 shows the distribution of experimental events as the functions of the $Cos\theta^{\gamma}$ variable. Theoretical curves have been obtained when determining the form factors $F_1^V(K^2)$ and $F_\pi(K^2)$ (see Table 1) by using the dispersion model.

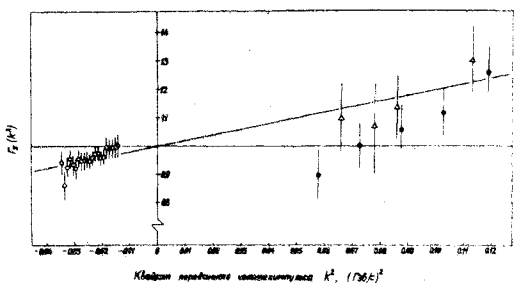

Fig.2. Results of pion formfactor measurements/8/ in experiments on pion scattering on electrons ($K^2<0$) and in the experimental studies of the $\pi^-p\to e^+e^-n$ process ($K^2>0$): ▲ –/2/, Δ –/3/, ● – the present investigation. Solid curve is the result of calculations in the superpropagator model/9/.

The data were ($\chi^2=13.7$ with $\overline{\chi^2}=4$) approximated by the function $F_1^V(K^2)=1+1/6\,\bar{z}^2K^2$ with $\bar{z}=\bar{z}_\pi=0.75\pm0.09$ f.

For the part of statistics the phenomenological analysis of data on reaction (1) is presented. It allowed to determine the contributions of states with various photon polarizations to the IEP differential cross section. In one-photon approximation the IEP cross section is written as/5/

$$\frac{d\sigma}{d\Omega_\gamma\, d\Omega_e\, dK^2}=\sum_{i=1}^{4}R_iT_i=\sum_i\sigma_i, \qquad (2)$$

where K^2 is the square of the 4-momentum transferred, Ω_e, Ω_γ are solid angles of gamma-quantum and electron scattering, i is the index determining photon polarization, T_1 describes the process

$$\pi^-p\to\gamma^*+n \qquad (3)$$

with transverse nonpolarized virtual gamma-quanta, T_2 corresponds to processes with transversely polarized photons, T_4 corresponds to processes with longitudinally polarized photons, T_3 describes interference longitudinally and transversely polarized photons, σ_i corresponding differential cross section, the coefficient R_i is the known functions of variables K^2, $Cos\varphi$, and $Cos\theta_e$.

The particular form of the parameter T_{1-4} depends upon the applied theoretical model. In the phenomenological analysis the two-dimensional distribution of IEP events of the variables $Cos\varphi$ and $Cos\theta_e$ was approximated by function (2) with varied parameters T; the coefficients R_i as functions of variable $Cos\varphi$ and $Cos\theta_e$ were calculated by the Monte-Carlo method with the account of real experimental conditions. All the experimental statistics was distributed into five groups on K^2 with average values of equal to 1.48 f^{-2}, 1.88 f^{-2}, 2.26 f^{-2}, 2.65 f^{-2}, 3.05 f^{-2}. For each group the phenomenological analysis was performed. The obtained evaluations are shown in Fig.3 (a,b,c). The same Figs. show the results of theoretical calculations (solid curve). It is seen that the model/6/ well des-

cribes the behaviour of cross sections corresponding to the radiation of the transverse nonpolarized and longitudinal photons.

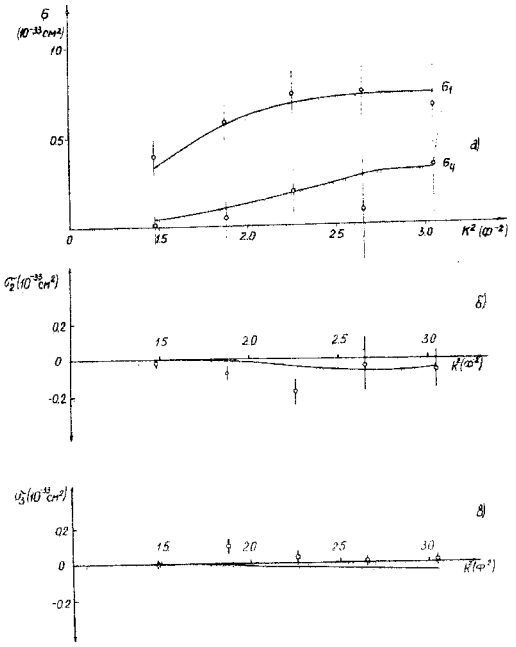

Fig.3

As has been shown by calculations, the σ_1 cross section depends equally on the Dirac isovector formfactor F_1^V of the nucleon and the pion formfactor F_π. The value of σ_4 depends, mainly, upon F_1^V: the variation of F_1^V within 10% changes σ_4 by 14%,2%, while a 10% change of F_π changes σ_4 only by 3.8%. Thus if the value of σ_4 is known with a small error, F_1^V can be determined with a good accuracy even when a rough estimation of the formfactor F_π is used. Since σ_4 is determined only by Born terms[6], the obtained value is not dependent upon model uncertainties.

References

1. Yu.K.Akimov, L.S.Vertogradov, A.V.Demyanov et al. Yad.Phys., 13, 748 (1971).
2. S.F.Berezhnev, L.S.Vertogradov, A.V.Demyanov et al. Yad.Phys., 16, 185 (1972).
3. S.F.Berezhnev, A.V.Demyanov, A.V.Kulikov et al. Yad.Phys., 18, 102 (1973).
4. S.F.Berezhnev, T.D.Blokhintseva, A.V.Demyanov et al. JINR, P1-9575, Dubna, 1976.
5. Yu.S.Surovtsev, F.G.Tkebuchava. JINR,P2-4524, Dubna, 1969.
6. T.D.Blokhintseva, Yu.S.Surovtsev, F.G.Tkebuchava. Yad.Phys., 21, 850 (1975).
7. G.Adylov, F.Aliev, D.Bardin et al. Phys.Lett., 51B, 402 (1974).
8. M.K.Volkov, V.N.Pervushin. Nuovo Cim., 27A, 277 (1975).

MEASUREMENT OF THE PION FORM FACTOR*

E.Dally, J.Hauptman, C.May, D.Stork
University of California at Los Angeles

J.Poirier, C.Rey, R.Wojslaw
University of Notre Dame

P.Shepard
University of Pittsburgh

A.Lennox, J.Tompkins, T.Toohig, A.Wehmann
Fermi National Accelerator Laboratory

I.Ioan, T.Nigmanov, E.Tsyganov, A.Vodopianov
Joint Institute for Nuclear Research, Dubna

The pion form factor has been measured in the momentum transfer range $0.03 \leq q^2 \leq 0.07$ $(GeV/c)^2$ by scattering pions from atomic electrons in a liquid hydrogen target. The pion form factor is defined to be the elastic scattering cross section divided by that predicted for a point pion. When it is expanded in powers of q^2, the mean-square radius of the pion electromagnetic charge distribution appears in the first coefficient:

$$\frac{d\sigma}{dq^2} = \left(\frac{d\sigma}{dq^2}\right)_{\substack{\text{POINT}\\ \text{PION}}} \left|F(q^2)\right|^2$$

The experiment was performed in a 100 GeV/c negative pion beam incident on a 50 cm liquid hydrogen target at Fermilab. The maximum recoil electron energy is 84.0 GeV which corresponds to a maximum momentum transfer squared in the elastic reaction of $q^2 = 2m_e(E_e - m_e) = 0.086$ $(GeV/c)^2$. These small momentum transfers give laboratory scattering angles which are typically a few milliradians within our acceptance. The trajectories of the incident pion and of the scattered pion and electron are measured with proportional wire chamber stations, each having four planes with 2 mm wire spacing staggered by 1 mm. The scattered particles are bent through two BM109 magnets with a total field integral of 70.35 Kg-m, and their trajectories beyond the magnets are measured by six magnetostrictive wire spark chambers.

Downstream of the spark chambers is a two particle trigger hodoscope. The geometric efficiency for triggering is nearly 100% for the range $0.03 \leq q^2 \leq 0.07$ $(GeV/c)^2$. An array of ten lead-glass shower counters 14 radiation lengths long served to reduce background triggers during the run and to aid in the subsequent identification of elastic pion-electron events. Scattered muons were identified with a segmented steel filter.

An event trigger required conditions of two distinct types: the first was a beam monitor signal defining the incident pions. The beam logic was composed of information from scintillation counters and the proportional chambers upstream of the hydrogen target. A portion of the beam logic required one and only one beam particle incident on the hydrogen target. This logic demanded a 1 microsecond spacing between usable particles; it vetoed beam counts with two particles in one r.f. bucket or with a particle in the following bucket. These requirements limited the amount of usable beam per machine pulse (typically, 300 K particles through the spectrometer of which about 100K were usable for the experiment), but created a clean environment for spectrometer operation which removed serious ambiguities and inefficiencies from the trackfinding procedure.

The second trigger logic condition defined the pion-electron scatter: a two particle signature from the proportional chambers downstream of the target, a two particle signal from a scintillation counter array behind the spark chambers, and a Čerenkov pulse height consistent with that expected from the scattered electron. The trigger rate during data taking was about 1.4×10^{-4} per incident pion, and about 15 events were recorded during the 1 second machine spill.

The geometrical event reconstruction was done by finding tracks in the horizontal and vertical planes, and matching them in rotated chambers. The efficiency of pion-electron event finding has been tested both by Monte Carlo simulation of the experiment and by a second, independent program, and found to be 99.0 ± 1.0 % in this sample of data. A distribution of the reconstructed vertex position for elastic events is shown in Figure 1.

* Supported in part by U.S.Energy Research and Development Administration and the National Science Foundation.

The pion-electron elastic scatters are separated from the large hadronic background by employing four constraints of energy-momentum conservation, and by requiring that the energy deposited in the leadglass shower counters be consistent with the momentum measured in the spectrometer of the showering particle. Constrained chi-squared fits were performed on the spectrometer data for the pion-electron elastic reaction with an additional external bremsstrahlung photon assumed to be along the electron direction. The χ^2 distribution for this three-constraint reaction hypothesis on the present sample of data is shown in Figure 2; the tail on this distribution has contributions both from strong interaction background and from real pion-electron elastic scatters. A relatively large number of pion electron elastic events (about 3%) in this sample exceeds the statistical 1 % confidence level (at χ^2=11.5 for three constraints), and these are accounted for by vertex associated radiative effects, pions which nuclear elastic scatter in the target or the spectrometer matter, pions which decay inside the spectrometer, the non-gaussian distributions associated with plural scattering in thin absorbers, and systematics of the geometrical event reconstruction. The fitted bremsstrahlung spectrum is shown in Figure 3; the insert shows the spectrum near zero photon energy. The normalized and calibrated Čerenkov pulse height spectrum for kinematically identified elastic events is displayed in Figure 4.

The final separation of the elastic events from the background employs the geometry of event reconstruction in the target, the kinematic χ^2 from the constrained fit to elastic kinematics, a cut on the fitted bremsstrahlung energy at 4 GeV, and a minimum shower counter pulse height for electron identification. Specifically, we demand that the confidence level of the kinematic fit exceed the 10^{-6} level, that the shower counter pulse height exceed 50% of that expected for the electron, that the reconstructed vertex position be within 30 cm of the target ends, and that the kinematically fitted photon energy be between -2.0 and 4.0 GeV.

To obtain the form factor from the measured distribution in q^2 of elastic events, corrections for many physical and instrumental effects must be made. The principal corrections affecting the incident pion flux are pion attenuation in the target and spectrometer matter (2.87%), beam momentum cut from 96 to 102 GeV/c (3.02%), and muon contamination (0.40%). Principal corrections affecting the elastic sample of events are bremsstrahlung of the electrons (15% to 20%), pion attenuation (4.63%), and radiative corrections[1] (7.9% to 9.3%). The pion decay, muon-electron scattering, and strong interaction background corrections are less than 1%. Trackfinding efficiency was found to be 99%, and geometrical efficiency varied from 95.25% to 99.47%.

The corrected form factor is shown in Figure 5. At the present time a simple least squares fit which neglects error correlations has been carried out on this sample of data in order to provide a preliminary value for the pion radius. The fit is constrained in overall normalization to correspond to a 2 percent uncertainty in the absolute cross section. We find

$$\langle r_\pi^2 \rangle = 0.33 \pm 0.06 \text{ f}^2.$$

For comparison, vector dominance predicts 0.40 f^2, and the size of the proton is 0.66 f^2. The first direct experimental determination[2] obtained $0.61 \pm .15$ f^2.

We express our appreciation to the staff of Fermilab for their assistance throughout this experiment. Dr. Charles Buchanan contributed to the preparation for the experiment, and Mr.Jonathan Kubic and Mr.Jim Volk were of great help. We are grateful for the support and encouragement of Dr. E.Goldwasser and Dr. A.Baldin.

References

1. D.Yu.Bardin, G.V.Micelmacher, N.M.Shumaiko. JINR E2-6235 (1972).
2. Adylov et al., Physics Letters 51B, 402 (1974).

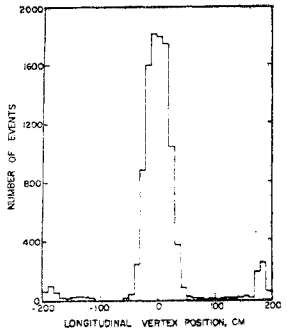

Fig.1. The reconstructed vertex position in 10-cm bins of identified elastic scatters in the neighborhood of the 50-cm liquid hydrogen target. The ends of the vacuum region and the PWC stations 2 and 3 are visible.

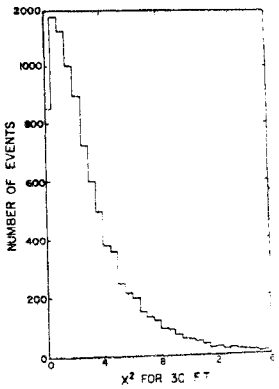

Fig.2. The three-constraint chi-squared distribution for constrained chi-squared fits to the elastic reaction with an assumed bremsstrahlung photon along the electron direction .

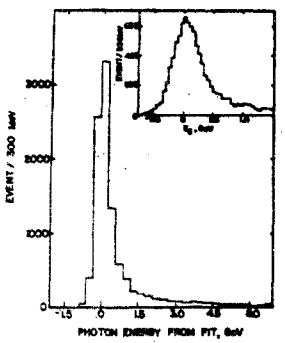

Fig.3. The fitted bremsstrahlung spectrum for elastic events, with an insert showing this distribution near zero photon energy. The mean of this distribution is consistent with the known amount of matter which the scattered electron tranverses.

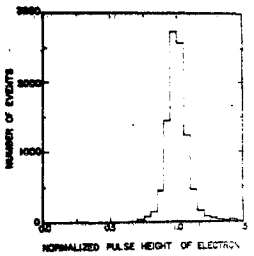

Fig.4. The momentum normalized shower counter pulse height spectrum for elastic events.

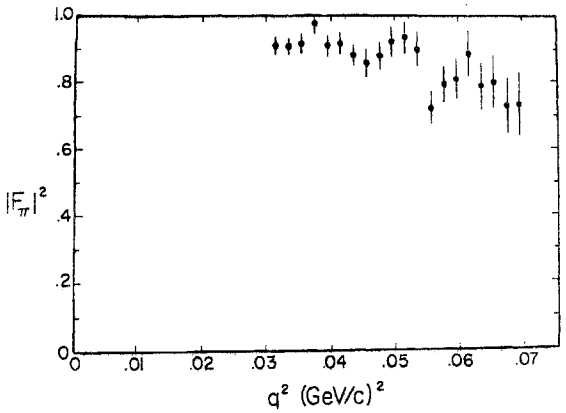

Fig.5. The pion form factor.

PHENOMENOLOGICAL ANALYSIS AND THE MODELS OF THE ELECTROMAGNETIC FORM FACTORS OF HADRONS

N.B.Skachkov
Joint Institute for Nuclear Research, Dubna

Nowadays the center of the interests in studying the structure of elementary particles has removed to studying the information which is contained in the experimentally observed behaviour of the structure functions of inelastic processes. But it does not mean that the problem of understanding the physics controlling the elastic form factors fall off is solved. This problem remains to be still interesting and it is the subject of a number of papers presented at this conference.

In /1/ a new formula was obtained for the proton form factor (f.f.)

$$F_p(t) = \frac{y}{\sinh y} \cdot \sum_{V=\rho,\omega,\varphi,\rho''(1650)} \frac{a_V}{\mu^2 - t} \qquad (1)$$

(y - is the rapidity, corresponding to the square of the 4-momentum transfer $t=(p-k)^2$: $y = Ar\cosh\left(\frac{2M^2-t}{2M^2}\right)$, M - proton mass). Formula (1) gives the correct, almost dipole asymptotical behaviour of the proton f.f.

$$F_p(t) \approx \frac{2M^2 \ln\frac{|t|}{2M^2}}{t^2}, \quad -t \gg 4M^2 \qquad (2)$$

The factor $y/\sinh y$ in (1) takes into account the contribution of the central part of the proton (with $R = 1/M$), because, as it was established in /1/, by passing to the relativistic configurational representation (RCR), the $\rho,\omega,\varphi,\rho''(1650)$ mesons produce the proton structure only at distances beyond the proton Compton wave length. The relativistic configurational representation was introduced in /2/ by using instead of the conventional Fourier analysis the expansion on the Lorentz group. For the form factor this transition looks like /1/

$$F(t) = 4\pi \int_0^\infty \frac{\sin rMy}{rM\sinh y} F(r) r^2 dr. \qquad (3)$$

The group parameter r in (3) enumerates the eigenvalues of the Casimir operator of the Lorentz group $\hat{C}_4 = \frac{1}{4} M_{\mu\nu} M^{\mu\nu}$ ($M_{\mu\nu}$ generators of the Lorentz group)

$$\hat{C}_4 \left(\frac{\sin rMy}{rM\sinh y}\right) = \left(\frac{1}{M^2} + r^2\right)\left(\frac{\sin rMy}{rM\sinh y}\right)$$

In (3) the parameter r plays the role of the relativistic generalization of the relative coordinate.

Due to the modulus of the new coordinate r is the relativistic invariant and the expansion (3) holds in any reference frame, the distribution function $F(r)$ in this new coordinate space is also invariant and describes the particle structure in any reference frame (and not necessarily in the Breit frame as usual).

The relation that expresses the mean-square radius through a new coordinate plays an important role for the model. Let us mention first that to give the interpretation to the formal definition of the invariant mean-square radius $\langle r_0^2\rangle = 6\frac{\partial F(t)}{\partial t}\Big/_{t=0}$ one usually passes to the Breit frame ($\vec{p} = -\vec{k}$; $t = -(\vec{p}-\vec{k})^2 = -2\vec{p}^{\,2}$), where it coincides with the eigenvalue of the Casimir operator $\hat{C}_E$ of the motions group of the three dimensional Euclidean momentum space $\hat{C}_E = \left(i\frac{\partial}{\partial \vec{q}}\right)^2$: $\hat{C}_E\, e^{i\vec{q}\vec{r}} = r^2 e^{i\vec{q}\vec{r}}$

$$\langle r_c^2\rangle_{Br.fr.} \equiv -6\frac{\partial F(t)}{\partial \vec{q}^{\,2}}\Big/_{\vec{q}^{\,2}=0} = \left\{\hat{C}_E F(t)\right\}\Big/_{\vec{q}^{\,2}=0}$$

In /1/ it was shown that the invariant mean-square radius also has the group-theoretical meaning namely, it is the eigenvalue of the Casimir operator of the Lorentz group

$$\langle r_0^2\rangle \equiv 6\frac{\partial F(t)}{\partial t}\Big/_{t=0} = \left\{\hat{C}_4 F(t)\right\}\Big/_{t=0}. \qquad (4)$$

From (3) and (4) the expression follows for an invariant mean-square radius through the invariant distribution $F(r)$ in a new coordinate space:

$$\langle r_0^2\rangle \equiv 6\frac{\partial F(t)}{\partial t}\Big/_{t=0} = \frac{1}{M^2} + \frac{\int r^2 F(r)\, d^3\vec{r}}{\int F(r)\, d\vec{r}}. \qquad (5)$$

We see that when the distribution $F(r)$ is of constant sign, a new coordinate r and $F(r)$ describe only the distance beyond the Compton wave length $\frac{1}{M}$ $(\hbar = c = 1)$.

If we analyze the VDM model of the electromagnetic form factors in terms of a new coordinate space then we shall find that in this space the transform $F(r)$ of a meson propagator $\frac{1}{\mu_V^2 - (p-k)^2}$ essentially depends on the relation between the mass M of the particle itself and that of the intermediate vector meson μ_V: $F(r)$ is the function of the constant sign when $\mu_V^2 < 4M^2$ and alternative function when $\mu_V^2 > 4M^2$ /2/. The recently discovered vector mesons ϱ, ω, φ and ϱ'' (1650) satisfy the first relation $\mu^2_{\varrho,\omega,\varphi,\varrho''} < 4M_p^2$, thus they contribute the proton structure only at distances beyond its Compton wave length $1/M_p$. So, to reflect the whole proton structure in the momentum space, we need to add the contribution of the central part with $\langle r_c^2 \rangle = 1/M_p^2$. From (5) it follows that to the central sphere with $\langle r_c^2 \rangle = 1/M^2$ there corresponds the spatial distribution $F(r) = \frac{\delta(r)}{4\pi r^2}$. According to (3) it provides the contribution to the form factor $F(t)/_{r_c = 1/M} = y/\sinh y$ that modifies the VDM for the proton f.f. by formula (1).

From the view-point of quark models the obtained picture may be interpreted as follows. According to the estimate by these models /3/, the relative motion of three quarks constituting a proton is within the region of the proton Compton wave length order. Consequently, they produce the contribution of the central part of a proton, while the quark-antiquark pairs compose the vector mesons, responsible at $\mu_V^2 < 4M_p^2$ for the distribution at distances beyond $1/M_p$.

The results of fitting of experimental data by formula (1) are given in /4/. In /4/ at account of 84 data points with approximately equal number of data points at $-t < 1$ GeV^2 and $-t > 1$ GeV^2 the obtained value of χ^2 per degree of freedom was $\chi^2_{deg.fr.} = 1.04$. The fitting of the whole world experimental data (299 points) performed in /5/ gave $\chi^2_{deg.fr.} = 1.21$ with the confidence level C.L.=1%, while in this case the usual VDM gives C.L.=0.03–0.1%. Besides formula (1), that was obtained in 1974 /1/ when "the measured form factor seems to fall faster than $1/q^4$ " /6/, predicted that at asymptotical $-t \gg 4M_p^2$ the decrease of the f.f. should be more slow than t^{-2} up to the factor $\ln \frac{|t|}{M^2}$ in /2/. The quark counting rules /7/ also give the proton decrease as t^{-2}. The last experiments in 1975 have shown that really at $-t \geq 25$ GeV^2 the decrease becomes slower than t^{-2} (see Fig.1

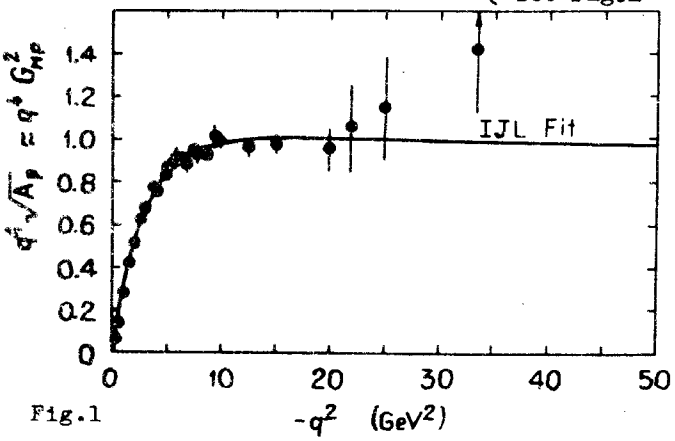

Fig.1

and prof.Chertok's talk also).

The problem of description of electromagnetic form factors in the framework of the dispersion approach was discussed in /8/. The authors also took into account the $\pi\omega$ state beside the $\pi\pi$ intermediate state. The analyticity and unitarity lead to the following system of equations (see Fig.2).

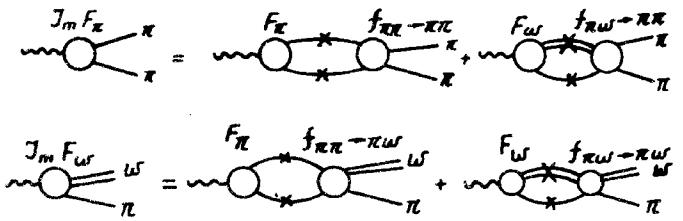

Fig.2

These relations allow to determine by a model independent way the F_π and f.f. F_ω of $\gamma \to \pi^0\omega$ transition by phase of $\pi\pi$ and $\pi\omega$ scattering and inelasticity. The relation obtained enables with the use of the data to conclude that the phase shift of $\pi\omega$-scatter-

ing goes through $\pi/2$ in the region of the ρ' (1250) resonance. By taking into account the ρ and ρ' with $\frac{g_{\rho'\omega\pi}}{g_{\rho\rho\pi}} \cdot \frac{g_{\rho\pi\gamma}}{g_{\rho'\omega\pi}} \approx \frac{1}{2}$ the authors succeded in the description of data on F_ω (fig. 3) and F_π (fig. 4) the $\Gamma_{\rho'\to 2\pi}$ being approximately close to zero.

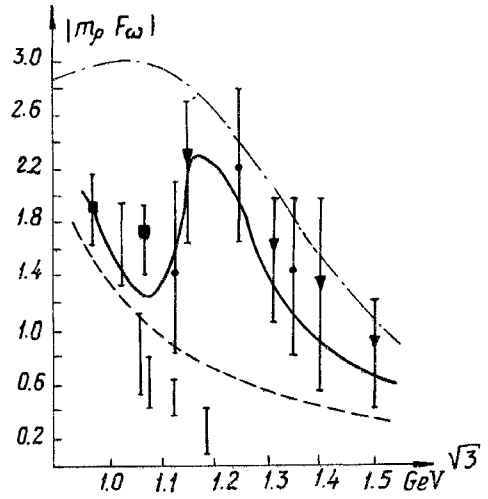

Fig.3

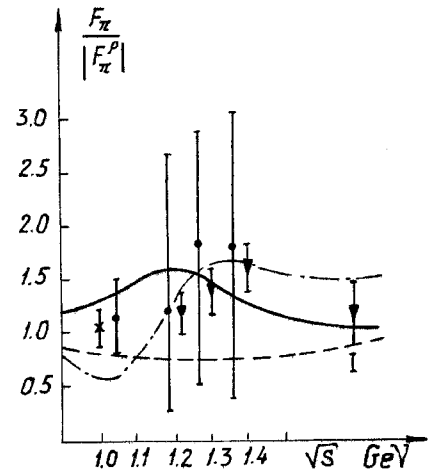

Fig.4

The remarkable property of these relations is that the data on $F_\pi(s)$ at $t>0$ are satisfactory described too (fig.5).

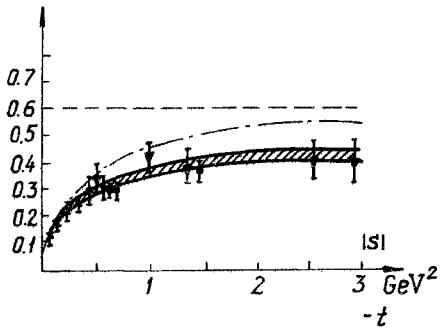

Fig.5

The authors of /9/ have analyzed the pion f.f. data in the time-like region to find out the possibly existing ρ' and ρ'' resonance structures in these data. They have shown that with the restriction $\chi^2_{deg.fr.}=0.5$ 3 resonance structures can be distinguished in the Argand diagram at 1280 MeV (ρ' - meson region), 1510 MeV (ρ'' meson region) and at 1920 MeV. But with $\chi^2_{deg.fr.}$ increasing up to $\chi^2_{deg.fr.}=0.6$ only one resonating structure at 1510 MeV remains. So they conclude that the only feature that can be clearly extracted from nowadays data is a resonance at ρ'' 1500-1600 MeV region.

The problem to describe electromagnetic properties of hadrons on the basis of strong interaction data is also dealt within paper /10/. In this paper an integral representation is used expressing form factors of two-particle systems in terms of phase shifts of strong interaction between the constituent particles and their f.f.. Such an approach is manifestly covariant and is shown to yield the results usually obtained with the use of phenomenological potentials in the nonrelativistic limit. As example the authors present the deuteron's charge form factor. Their method when applied to the nucleon form factors shows that the magnetic f.f. should decrease faster than the electric one at large $-q^2$:

$$G_{E_{n,p}}(q^2) \sim G_E^V(q^2) \sim \frac{F_\pi(-q^2)}{\sqrt{-q^2}} \cdot \sin\delta_{11}(-q^2)$$

$$G_{M_{n,p}}(q^2) \sim G_M^V(q^2) \sim \frac{F_\pi(-q^2)}{(-q^2)\sqrt{-q^2}} \cdot \sin\delta_{11}(-q^2)$$

δ_{11} is the phase shift of the πN - scattering.

In paper /11/ it was shown that the measurements of asymmetries in the elastic scattering of longitudinally polarized leptons on a polarized proton target at high $-q^2$ makes it possible to distinguish between two possible relations for the proton f.f.

$$F_1(q^2) \sim F_2(q^2) \qquad \text{I}$$

or

$$G_E(q^2) \sim G_M(q^2) \qquad \text{II}$$

at large $-t$. The I case is realized in composed model based on the Bethe-Salpeter equation, the case II follows from standard parton model, asymptotically free theories and, as it was shown in /12/, also holds in theories with γ_5, or chirality invariance, proposed in /13/. In /11/ it is shown that in I case, that still cannot be excluded by available experimental data at high $-q^2$, the longitudinal $A_{\parallel}$ and transverse $A_{\perp}$ asymmetries behave similarly (fig.6) $A_{\parallel} \sim A_{\perp}$

while in the II case (fig.7)

$$|A_{\parallel}| \gg A_{\perp}$$

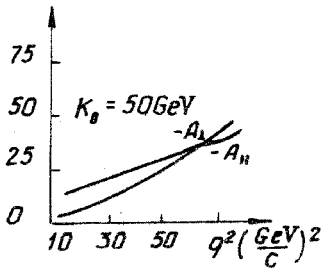

Fig.6

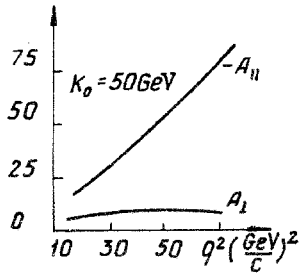

Fig.7

The experimental check of these relations will be a very powerful test of our understanding of proton structure.

The electroproduction of baryon resonances in the first, second and third resonance regions are analyzed in /14/ within the framework of the relativistic quark model. Current matrix elements are constructed on the three-dimensional surphase, defined by Markov-Yukawa conditions. The obtained results are in good agreement with experiment in a wide range of transfer momentum.

References:

1. N.B.Skachkov. JINR preprints E2-7890; E2-8424, Dubna, 1974; E2-8857, Dubna, 1975; Soviet Journal Theor.and Math.Phys. 23, N.3. (translation of Theor.i Mat.Fiz. 23, N.3 (1975) 313).
2. V.G.Kadyshevsky, R.M.Mir-Kasimov, N.B.Skachkov. Nuovo Cim. 55A (1968) 233; Soviet Journal of Particles and Nuclei (translation) 2, N.3 (1972) 69.
3. S.B.Gerasimov. JINR preprint P-2439, Dubna, 1965; P-2619, Dubna, 1966. A.D.Licht, A.Pagnaments. Phys.Rev. D2, 1150 (1970).
4. N.B.Skachkov, I.L.Solovtsov. JINR preprint E2-9504, Dubna, 1976.
5. S.I.Bilenkaya, N.B.Skachkov, I.L.Solovtsev, Contribution 602/A7-13 at this Conference.
6. P.N.Kirk et al. Phys.Rev. D8, 63 (1973).
7. V.A.Matveev, R.M.Muradyan, A.N.Tavkhelidze. Nuovo Cim. 7,719 (1973); S.J.Brodsky, G.R.Farrar. Phys.Rev.Lett. 31, 1153 (1973).
8. N.M.Budnev, V.M.Budnev, V.V.Serebryakov. Novosibirsk Math.Inst. preprints T - 88, T - 89 (1976).
9. C.B.Lang, I.Sabba-Stefanescu. Univ.of Karlsruhe TKP 14/75 (1975).
10. A.I.Kirillov, V.E.Troitski, Yu.M.Shirokov. Contribution 597/A7-31 at this section.
11. S.I.Bilenkaya, S.M.Bilenky, A.Frenkel, E.H.Hristova. JINR preprint E2-8678, Dubna (1975).
12. B.L.Ioffe. ITEF-preprint ITEP-50, Moscow, 1976.
13. A.A.Logunov, V.A.Meshcheryakov, A.N.Tavkhelidze, Dokl.Acad.Nauk SSSR 142, 317 (1962).
14. A.P.Kobushkin, Yu.M.Sinjukov. Contributions 596/c@-6; 598/C4-8 at this conference. V.F.Dushenko, A.P.Kobushkin, Y.M.Sinjukov. Soviet Journal Nucl.Phys. 24, 434 (1976).

VECTOR MESON-NUCLEON COUPLING CONSTANTS

G. Höhler

Institute for Theoretical Nuclear Physics,
Karlsruhe University, FRG

1. ρ NN Coupling Constants (Ref. [1]).

An investigation of the $I=J=1$ $\pi\pi NN$ partial waves offers the best possibility for a determination of the properties of the ρNN vertex. Following Frazer and Fulco [2] one has to perform two analytic continuations in order to obtain from πN amplitudes the partial waves in the region of interest.

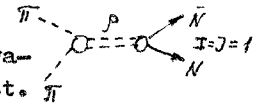

i) The partial waves $f_i(t)$ at $t<0$ $(i=1,2)$ follow from a projection of πN amplitudes which are continued at fixed t to the region between the s- and u-channels in the Mandelstam diagram. The continuation is trivial, since we have used Pietarinen's new phase shift analysis [3] which incorporates fixed-t analyticity from the beginning.

ii) Continuation of the partial waves $f_i(t)$ to the t-region of the ρ-peak. A reliable continuation is possible only, because the phase of $f_i(t)$ can be taken from the p-wave $\pi\pi$-phase shift and also from a fit to the data for the pion form factor $F_\pi(t)$.

It is assumed that the 4π contribution to the extended unitarity relation can be ignored up to the $\omega\pi$ threshold, because 4π-production in $\pi^+\pi^-$ and e^+e^- is negligible in this range.

Because of the large ρ-width the value of the coupling constant depends to some extent on its definition (Ref. [1]). Results for the vector and tensor ρNN coupling constants in Sakurai's convention:

$$f_V^2(\rho)/4\pi = 2.2. \qquad f_T(\rho)/f_V(\rho) = 6.6$$

The error is estimated to be of the order of 10% for f_V, f_T.

f_V is near to the usual value, f_T/f_V is much larger than the value 3.7 obtained with the simplest VDM model for the nucleon form factor. We believe that other methods have a larger uncertainty.

2. Other VNN Coupling Constants

In order to determine further VNN coupling constants we have used the dispersion method for a new analysis of the electron-nucleon scattering data [4,5]. The dispersion relation for the Dirac and Pauli form factors reads $(i=1,2)$

$$F_i(t) = \frac{1}{\pi}\int_{4\mu^2}^{\infty} \frac{\mathrm{Im}\, F_i(t')}{t'-t}\, dt' \qquad (2.1)$$

According to Frazer and Fulco the ρ-contribution to $\mathrm{Im}\, F_{iV}$ follows easily from the result of the calculation described in sect.1.

$$\mathrm{Im}\, F_{iV}(t) = \frac{q_t^3}{\sqrt{t}} F_\pi^*(t) f_i(t);\quad q_t^2 = \frac{t}{4} - \mu^2 \qquad (2.2)$$
$$t \le 50\mu^2$$

All other contributions are described by pole terms

$$\mathrm{Im}\, F_{iV} = \mathrm{Im}\, F_{iV}^{\rho} + \pi \sum_V a_i(V)\, \delta(t-t_V);\quad V = \rho, \rho', \rho'' \ldots \qquad (2.3)$$

$$\mathrm{Im}\, F_{is} = \pi \sum_V a_i(V)\, \delta(t-t_V);\quad V = \omega, \phi, \omega' \ldots$$

In order to demonstrate that the accurate result for $\mathrm{Im}\, F_{iV}$ differs significantly from a pole approximation, we show a figure for the integrand of the dispersion integral for $F'(0)$, from which the isovector nucleon radius is determined [4]. The enhancement just above $t = 4\mu^2$ is caused by a logarithmic singularity of $F_{iV}(t)$ in the 2nd sheet at $t = 3.98\mu^2$, which belongs to the contribution of the perturbation graph.

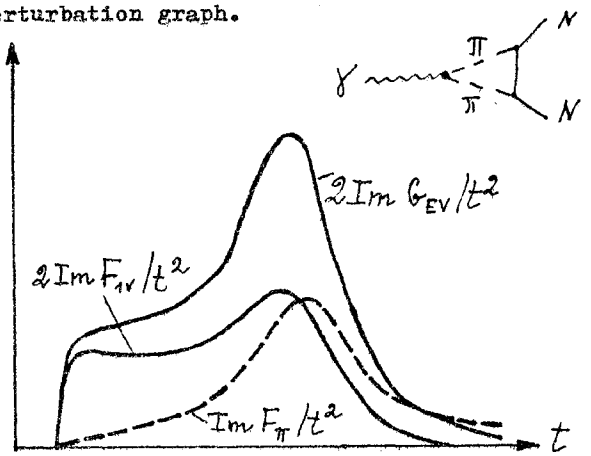

The enhancement is not present in the pion form factor. Therefore its t-dependence must be different from that of F_{1V}, contrary to the assumption in several papers.

The VNN coupling constants $g_i(V)$ follow immediately from the results for the residues

$$a_i(V) = \frac{m_V^2}{f_V} g_i(V) \quad (2.4) \qquad \frac{m_V^2}{f_V} = \frac{1}{z_V \cdot t}$$

since the γV coupling constants are known from $e^+e^- \to V$ experiments. In order to have a simple notation, we are using now half of the earlier $\rho\bar{N}N$ coupling constants: $g_i(\rho) = f_i(\rho)/2$.

Input Data: all accurate $ep \to ep$ cross sections, $en \to en$ cross sections from ed-data, $e^+e^- \leftrightarrow \bar{p}p$ data. $G_{En}'(0)$ from the scattering of slow neutrons against atomic electrons (New data: [6]). Our result is consistent with the $\pi^- p \to e^+e^- n$ data of the Dubna group [7]. Since it is difficult to determine the Dirac isovector form factor and the pion form factor separately, it would be useful to analyse the data with the constraint that the difference $Re\,2F_{1V} - Re\,F_\pi$ and the imaginary parts are taken from our results.

Adjustable Parameters: all $a_i(V)$, the masses of the pole terms (except ω, ϕ). These masses were restricted to lie beyond 1 GeV. The normalizations of the eN-scattering data (in general within the errors given by the authors).

The problem is not well defined without a simplicity condition. We restricted the oscillations by demanding that $\sum_V |a_i(V)|$ should not be much larger than the minimum value necessary for a good fit $(\chi^2_{DF} \approx 1)$

Results

1. $ep \to ep$ data only

It is interesting to find the number of parameters which can be determined in a reliable way

Usual dipole fit, normalization of data as published 11.6
the same, but normalizations adjusted . . . 4.3

Best fit (298 data points, 5 parameters in the ansatz, normalizations adjusted) 0.9

2. All Data

In this case our best fit has $\chi^2_{DF} = 1.3$, the number of adjustable parameters in the ansatz being 8.

The main effects are large bump-dip structures in $Im\,F_{1S}$ and $Im\,F_{2V}$. $Im\,F_{1V}$ is not far from ρ-dominance, $Im\,F_{2S}$ is small.

F_{2V}. The large ρ-peak is followed by a dip of almost the same area. Its position is near to the mass of the first daughter $\rho'(1250)$ of the ρ according to the Veneziano model. Part of the dip could be due to the tail of the ρ and the effective pole could be a description of a broad structure. If one attempts to shift the dip to the 1600 MeV mass region, the fit develops huge oscillations at larger t and becomes unacceptable. It was reported at this Conference that $\rho'(1250)$ is not seen in $e^+e^- \to \pi^0\pi^0\pi^+\pi^-$ up to 1.3 GeV Ref. [8]. This point deserves a further study, taking into account the results of Budnev et al. [9].

A crude estimate of the $\rho'NN$ tensor coupling constant gives $g_2^2(\rho') \approx 0.5\, g_2^2(\rho)$. There is no evidence for a structure at 1600 MeV, but this might change when better $e^+e^- \leftrightarrow \bar{p}p$ data give stronger restrictions for the spectral functions in the unphysical region.

F_{1S}. Since the OZI rule predicts a decoupling of ϕ from $\bar{N}N$, we started with an

ω – pole + 2 poles with adjustable masses. It turned out that one of the poles chose a mass near to the ϕ-mass. So we fixed this pole at m_ϕ. Our best solution has a fairly large vector coupling

$$g_1^2(\omega)/4\pi = 24 \pm 5 \pm 7.$$

The errors belong to f_ω and $a_1(\omega)$ respectively. Our results: $a_1(\phi)/a_1(\omega) = -0.9$, $g_1(\phi)/g_1(\omega) = -0.5$ clearly violate the OZI-rule. Therefore we have looked for other acceptable solutions.

It is easy to reduce the ϕ NN coupling by adding another pole in the 1200 MeV mass region. Up to now there is no evidence for a meson resonance $\omega'(1250)$, but it might be difficult to detect because of the large width due to $\omega' \to \rho\pi$ decay.

Since some symmetry predictions want a much smaller value of $g_1(\omega)$ (see below: $g_1^2(\omega)/4\pi = 3g_1^2(\rho)/4\pi \approx 5$), we have tried to find acceptable solutions with a smaller $a_1(\omega)$. It turns out that the fit wants to retain the magnitude of the bump. If we enforce a smaller $a_1(\omega)$ one obtains a large positive $a_1(\phi)$. The solution becomes unacceptable because of large oscillations at larger t, if we demand that both $a_1(\omega)$ and $a_1(\phi)$ are small.

3. SU(3) Relations Between VNN Coupling Constants (Ref. /10/)

SU(3) gives a relation between $g_i(\rho)$ and all other $V\bar{N}N$ coupling constants of the octet $(\rho, K^*, \bar{K}^*, \phi_8)$. In particular

$$g_i(\phi_8) = \frac{1}{\sqrt{3}}(4\alpha_i - 1) g_i(\rho). \qquad (3.1)$$

α_i is the $F/(F+D)$ ratio which is not determined by SU(3). $i = 1,2$ denotes vector and tensor coupling. The relation (3.1) is also valid for $i = E, M$, where

$$g_E = g_1 + \frac{m_v^2}{4m^2} g_2, \quad g_M = g_1 + g_2, \qquad (3.2)$$

m denotes the nucleon mass. In the VDM g_1, g_2 belong to the Dirac and Pauli form factors and g_E, g_M to the electric and magnetic Sachs form factors.

In order to obtain a relation for the physical couplings $g_i(\omega)$, $g_i(\phi)$ we insert the mixing relation

$$|\phi_8\rangle = \cos\theta\,|\phi\rangle + \sin\theta\,|\omega\rangle. \qquad (3.3)$$

The mixing angle is $\theta = 40^\circ$ if calculated from the Gell-Mann-Okubo mass formula. $\theta = 35.2^\circ$ is the quark model prediction ("ideal mixing").

We obtain for $i = 1, 2, E, M$

$$\frac{1}{\sqrt{3}\sin\theta}(4\alpha_i - 1)\frac{g_i(\rho)}{g_i(\omega)} - 1 = \cot\theta\,\frac{g_i(\phi)}{g_i(\omega)}. \qquad (3.4)$$

If the OZI-rule is fulfilled ($g_i(\phi) = 0$) and the mixing is ideal, we have $(4\alpha_i - 1)\,g_i(\rho) = g_i(\omega)$, i.e., $3g_i(\rho) = g_i(\omega)$ for pure F-coupling. If we compare our results with eq. (3.4), there are two simple possibilities for the assumption on the $F/(F+D)$ ratios:

i) We assume a pure F-type vector coupling, $\alpha_1 = 1$, as it follows, for instance, from Sakurai's conjecture that the interaction term in the Lagrangian is a product of the ρ-field and the isospin current ("ρ-universality"). Then eq. (3.4) agrees well with the $V\bar{N}N$ couplings of our best fit which violate the OZI-rule. The violation follows already from our large value of $g_1(\omega)$ as a SU(3) prediction from eq. (3.4). A possible $\omega'(1250)$ contribution must be small.

Another argument for a pure F-vector coupling starts from the fact that SU(3) leads to a pure F-coupling at t=0 for the matrix element of the electromagnetic current. Since ρ-dominance seems to be approximately valid for F_{1V}, there is a chance that this property remains valid up to $t = m_v^2$.

ii) Sugawara and von Hippel /11/ proposed that SU(3) should be applied to the couplings g_E and g_M and that the result for the $F/(F+D)$

ratios at t=0 remain valid up to $t = m_V^2$. Additional arguments were presented in a recent preprint by Gustafson [12]. Our results for g_E and g_M read

$$g_E(\rho)=5.5,\ g_M(\rho)=18.8;\ g_E(\omega)=16.9,\ g_M(\omega)=14.7$$

The assumption $\alpha_E = 1$ (pure F-coupling) is consistent with our values and the validity of the OZI rule ($g_E(\phi)=0$), since $g_E(\omega)=3g_E(\rho)$ There must be a large contribution from $\omega'(1250)$ exchange.

If we assume that ϕ decouples also in the magnetic case, we have for ideal mixing

$$(4\alpha_M - 1) = \frac{g_M(\omega)}{g_M(\rho)}$$

which gives $\alpha_M = 0.44$. The agreement with the SU(6) prediction 0.40 is good.

Aside from the fact that one needs a large contribution from ω' which has not been discovered, one would like to see a better justification, why the $F/(F+2)$ ratio at t=0 should remain valid up to $t = m_V^2$. The difficulty is that two exchanges ρ and ρ' give large contributions to $G_{EV}(0)$ and $G_{MV}(0)$. Furthermore the SU(6) prediction $G_{EN}(t)=0$ is wrong for small t, whereas $F_{EN}(t)=0$ is much nearer to the data.

Another possibility for a test of the OZI-rule was proposed by Gerasimov [13]. He studied relations between baryon form factors, in particular magnetic moments, taking into account SU(3) breaking but using unbroken SU(3) for the matrix element $\langle V | B\bar{B} \rangle$. The sign of the violation differs from ours.

4. Comparison with Other Determinations

Kravtsov et al. [14] used the optimal conformal method in order to determine new values for the nucleon radii. For the imput they used published form factors, taking into account normalization errors. The result is not much different from that of Ref.[15], deviations being probably due to the fact that the authors of Ref.[14] ignored the information on the spectral functions $Im\, F_{iV}$ from unitarity and also to the use of form factors instead of ep-cross section for the imput.

The information from unitarity has also been ignored in the work of Bilenkaja et al.[15] It will be interesting to compare the short range part of their spectral function with that of Ref. [15].

If our results for the VNN coupling constants are compared with those from other determinations, it is important to check whether the definitions of the coupling constants are the same. For instance authors working in NN-scattering give "$V\bar{N}N$ couplings at $t=0$", a notion which needs a more detailed explanations, since coupling constants are usually defined at $t = m_V^2$ (Ref.[16]).

In a paper presented by N.Zovko [17] the kaon radius was calculated in a low energy approximation to the unitarity relation for the $\pi\pi \to \pi\pi$ and $\pi\pi \to \bar{K}K$ amplitudes. The result is

$$F_K^V(q^2) = F_\pi(q^2).$$

References:

1. G.Höhler and E.Pietarinen, Nucl.Phys., B95 210 (1975).
2. W.R.Frazer and J.R.Fulco. Phys.Rev., 117, 1603 (1960).
3. E.Pietarinen, Nucl.Phys., B107, 21 (1976); preprint TKP 75/4 Un.of Karlsruhe, See also the talk of G.Oacles at this Conference.
4. G.Höhler and E.Pietarinen. Phys.Lett. 53B, 471 (1975).
5. G.Höhler et al. Preprint TKP 76/1. Papers 483 and I. Sabba-Stefanescu paper 104.
6. L. Koester et al. Phys.Rev.Lett., 36,1021 (1976).
7. S.F.Berezhnev et al. Yad.Fiz. 16, 185 (1972). and papers 1143,1144.
8. V.A.Sidorov , paper 639.
9. N.M.Budnev et al. Novosibirsk preprint TF 88.
10. H.Genz and G.Höhler. Phys.Lett. 61B, 389 (1976).
11. H.Sugawara and F.von Hippel . Phys.Rev. 145 1331, (1966); 172,1764 (1968).
12. G.Gustafson. Lund preprint (July, 1976).

13. S.B.Gerasimov, Paper 592.
14. A.V.Kravtsov and L.L. Nemenov, paper 1029.
15. S.I.Bilenkaya et al. Paper 602.
16. M.M.Nagels et al. Compilation of Coupling Constants and Low Energy Parameters, 1976.
17. N.Zovko, paper 364.

EFFECTS OF THE SU(3)-BREAKING IN MASSES AND ELECTROMAGNETIC DECAYS OF VECTOR MESONS

S.B.Gerasimov
Joint Institute for Nuclear Research, Dubna

Introduction

The breaking of the SU(3)-symmetry results in the mass shifts, modification of the interaction amplitudes and mixing of states belonging to different representations of the SU(3)-group. Various implications of the symmetry breaking in the vector meson sector came into focus of a particular attention when new data on the meson radiative decays have been obtained /1/.

Mass relations and mixing angles

From the conventional assumptions on the octet breaking of the SU(3)-symmetry and the singlet-octet configuration of the ω and φ meson

$$\omega = \omega_8 \sin\theta_V + \omega_1 \cos\theta_V \,, \qquad \varphi = \omega_8 \cos\theta_V - \omega_1 \sin\theta_V \,, \tag{1}$$

the GMO formula

$$4m^n_{K^*} - m^n_\rho = 3\left(m^n_\varphi \cdot \cos^2\theta_V + m^n_\omega \cdot \sin^2\theta_V\right) \tag{2}$$

follows. From the linear mass formula (n=1) one obtains $\theta_V \simeq 37^0$, while the quadratic one gives $\theta_V \simeq 39^0$. Introducing the symmetry breaking and the singlet-octet mixing into the "kinetic" rather than "mass" term of the Lagrangian results in the "current-mixing" scheme and the Coleman-Schnitzer /2/ mass formula, corresponding to $n = -2$ in Eq. (2) and $\theta_V \simeq 28^0$. So, it is necessary to refer to other sources of information to choose between different mass formulas and mixing angles.

Spectral function sum rules and the mixing angles

The spectral function sum rules (s.r.) follow from rather general assumptions on the unitary structure of the current commutators /3-5/. It was known for a long time that

the saturation of the 1-st Weinberg s.r. for the coserved vector currents (isospin I_μ^3 , hypercharge Y_μ and baryonic B_μ) by the ρ^0 , ω and φ - contributions gives the relation characteristic to the "current mixing" model /5/

$$tg\theta_B / tg\theta_Y = m_\omega^2 / m_\varphi^2 \qquad (3)$$

between angles θ_B and θ_Y , which define the vacuum-vector-meson matrix elements of the baryonic and hypercharge currents and related to θ_V in Eq. (1) via

$$tg^2\theta_V = tg\theta_B \cdot tg\theta_Y \quad . \qquad (4)$$

However, the lowest pole dominance assumption for the 1-st Weinberg s.r. within the SU(3)-symmetry appears to be too strong, as a sizeable deviation of the Das, Mathur and Okubo sum rule /4/ from experiment suggests. To have more reliable information on properties of the lowest vector mesons, it was proposed to consider a modified system of the spectral function sum rules in the broken nonet symmetry /6/

$$\rho_{-1}^{I_3 I_3} - \frac{3}{4}\rho_{-1}^{YY} = \frac{3}{2}\rho_{-1}^{BY} \quad , \qquad (5)$$

$$2\rho_{-1}^{BB} - \rho_{-1}^{YY} = \rho_{-1}^{BY} \quad , \qquad (6)$$

where

$$\rho_{-1}^{\alpha\beta} \equiv \int \frac{dm^2}{m^2}\rho^{\alpha\beta}(m^2) \quad , \qquad (7)$$

and, by construction, the integrals of the current spectral functions $\rho^{\alpha\beta}(m^2)$ over the high energy region are cancelled in Eqs. (5) and (6). Applying then (hopefully, more justified) the pole saturation to system (5) and (6) and using the (finite-width corrected) g_V -coupling constants ($V = \rho^0, \omega, \varphi$) /7/ we find two solutions:

$$tg\theta_B / tg\theta_Y \simeq \begin{cases} 1 & (8) \\ 0.3 & (9) \end{cases}$$

with the uncertainty of ± 0.1 for each value. The first solution (8) leads to single, universal, mixing angle $\theta_V = \theta_B = \theta_Y = 39^\circ \div 40^\circ$ which is in excellent accord with the quadratic GMO mass formula. The second solution results, via Eq. (4) and definition $tg^2\theta_Y = g_\varphi^2 / g_\omega^2$ in $\theta_V \simeq 23^\circ$, which is closer to 28° , given by the Coleman-Schnitzer mass relation. We should emphasize, however, that the conventional "current mixing" model gives relation (3) which does not coincide with either (8) or (9). We conclude therefore that the solution (9) might be connected with some different not yet well-recognized mixing scheme.

Radiative decays

Recent measurements of the meson radiative widths present serious difficulties for a number of popular theoretical models.

A. Quark model

The quark model description of the decays $V \to P\gamma$, $P \to V\gamma$ and (through the VDM) $P \to 2\gamma$, etc., has been discussed repeatedly /8/ . We add two remarks. First, assuming the universal SU(3)-breaking in the "strange" quark magnetic moment one can relate the established symmetry breaking in the Λ -hyperon magnetic moment to possible SU(3)-violation effects in the decays $K^* \to K\gamma$, $\varphi \to \eta\gamma$, $\eta(\eta') \to 2\gamma$. /9,10/. Note also that decrease in the transition magnetic moment $\mu(K^{*0}K^0)$ is accompanied by the increase of $\mu(K^{*\pm}K^\pm)$. Therefore, the comparison of the widths $\Gamma(K^{*0} \to K^0\gamma)$ and $\Gamma(K^{*\pm} \to K^\pm\gamma)$ should provide a critical check of the model.

The second remark refers to a possible strong breaking of the nonet symmetry for the pseudoscalar mesons. This effect can develop in a strong deviation from unity of the overlap radial integral $I_1 \equiv \langle 1|8\rangle_{rad.}$, when the singlet state is the pseudoscalar one. The numerical estimate of the I_1 can be obtained from the Schwinger mass formula /11/ . If

$\eta' = X(958)$, then $|\theta_p| \simeq 10^\circ$ and $L \simeq 0.5$. Alternatively, if we identify $\eta' = E(1420)$ [12], then $|\theta_p| \simeq 6^\circ$ and $L \simeq 1$. As far as $(L \cdot \sin\theta_p)_{\eta'=X} \simeq (L \cdot \sin\theta_p)_{\eta'=E}$ both hypotheses result in approximately the same value of $\Gamma(\eta \to 2\gamma)$. Clearly, $L < 1$ gives smaller values for the radiative widths of $\eta' = X(958)$. Some representative results of the quark model are given in Table 1 for the following set of parameters: $x = \mu(s)/\mu(d) = 2\mu(\Lambda)/\mu(N) \simeq 0.7$, $\theta_V = 39^\circ$, $\theta_p = -10^\circ$, $L = 0{,}5$. The widths of the $\rho \to \pi\gamma$ and $K^{*0} \to K^0\gamma$ decays may present difficulty for the model.

Table 1

Radiative decays of mesons

Decay mode	Theoretical models					Experiment
	1	2	3	4	5	
$\omega \to \pi^0\gamma$	input	790	850	870	824	870 ± 80 kev
$\rho \to \pi\gamma$	96±7	83	73	35	73	35 ± 10 kev
$K^{*0} \to K^0\gamma$	150±12	190	75	78	141	75 ± 35 kev
$K^{*+} \to K^+\gamma$	87±7	46	180	19	59	< 80 kev
$\varphi \to 2\gamma$	100±8	150	70	70	82	70 ± 16 kev
$\varphi \to \pi^0\gamma$	8.4±4.5	0.04	7.0	5.9	6.9 (input)	5.9 ± 2.1 kev
$\pi^0 \to 2\gamma$	input	7.2	6.3	3.0	6.7	7.92 ± 0.42 ev
$\eta \to 2\gamma$	0.36 ±0.02	0.36	0.0036	0.28	0.49	0.324 ± 0.046 kev
$X^0 \to 2\gamma$	1.3±0.1	6.0	5.3	12	–	< 19 kev
$X^0 \to \rho^0\gamma$	23±2	100	150	220	–	< 270 kev

1. The quark model ($\theta_V = 39^\circ$; $\theta_p = -10^\circ$; $L = 0{,}5$; $x = 0.7$).
2. The nonet symmetry ($\theta_V = 35^\circ$; $\theta_p = -10^\circ$) [13].
3. The nonet symmetry and the octet breaking of the SU(3) ($\theta_V = 35^\circ$; $\theta_p = -10^\circ$) [13].
4. The broken nonet symmetry ($\theta_V = 24^\circ$; $\theta_p = -10^\circ$) [15]
5. The generalized VDM and dynamical model of the SU(3) breaking ($\theta_V = 39^\circ$; $\theta_p = -10^\circ$) [16]

B. Phenomenological models

Within these models a certain unitary structure is assumed for corresponding vertices and free parameters are then found by fitting to available data [13–15].

a) Nonet symmetry and octet breaking of SU(3). The nonet symmetry dictates the following unitary structure for the $VP\gamma$ vertex

$$g(V^m P^i \gamma) = g_0 d_{min}\left(\delta_{n3} + \frac{1}{\sqrt{3}}\delta_{n8}\right), \quad (10)$$

where $m, i = 0, 1, 2, \ldots 8$. A general feature of all models using $\theta_V = 35^\circ \div 40^\circ$ is a strong disagreement of the $\rho\pi\gamma$-width with experiment [13–16] while the different models meet a different degree of success in describing the $K^* \to K\gamma$ decays. Taking account of the SU(3)-breaking via inclusion of the λ_8-spurion into Eq. (10), and using the "standard" angles $\theta_V = 35^\circ$ and $|\theta_p| = 10^\circ$ results in a very large value of the $K^{*+} \to K^+\gamma$ width [13], while a model, based on the generalized vector meson dominance, is somewhat hampered by the $K^{*0} \to K^0\gamma$ decay [16].

b) Broken nonet symmetry.

If only the nonet symmetry and not the SU(3) is broken, then three independent amplitudes describe all radiative transitions. In ref. [15] the value $\theta_p = -10^\circ$ was fixed, but θ_V was taken as a free parameter to be fitted by comparison with data. The value $\theta_V = 24^\circ$ was obtained, which is surprisingly close to that, resulting from solution (9) of the spectral function s.r. (5) and (6). This model gives satisfactory agreement with all the $V \to P\gamma$ decays [15] with an exception of the $\pi^0 \to 2\gamma$

width (assuming for the latter, as usual, the VDM model).

So, the $\varrho \to \pi\gamma$ decay appears like a key point in choosing between the symmetry breaking schemes. The accurate measurement of the $K^* \to K\gamma$ decays should be very important to check the SU(3). One can add also, that a useful information concerning the ω-φ mixing results from the $\omega\varphi$ - interference pattern in processes like $e^+e^- \to 3\pi, \pi^0\gamma$ /17/. The recent Orsay data /18/ seems to agree better with the mass-mixing models (i.e. when $\theta_V > 35^0$).

In conclusion, one cannot help stressing the extreme importance of (hopefully, soon and improved) new measurements of the $\varrho \to \pi\gamma$ and $K^* \to K\gamma$ decay widths.

REFERENCES:

1. C.Bemporad, in Proc. of 1975 Lepton-Photon Symposium, Ed. W.T.Kirk, Stanford, 1975, p.113. B.Gobbi et al., Phys.Rev.Lett., 33, 1450 (1974). W.C.Carithers et al. Phys.Rev.Lett., 35, 349 (1975).
2. S.Coleman, H.J.Schnitzer, Phys.Rev.,134, B 863 (1964).
3. S.Weinberg, Phys.Rev.Lett., 18, 507 (1967).
4. T.Das, V.S.Mathur, S.Okubo. Phys.Rev.Lett., 19, 470 (1967).
5. R.J.Oakes, J.J.Sakurai. Phys.Rev.Lett., 19, 1266 (1967).
6. S.B.Gerasimov. Communications of JINR P2-9020 (1975), and Paper No. 672.
7. J.LeFrancois, in Proc. of 1972 Leton-Photon Symposium, Cornell University, 1972.
8. G.Morpurgo, in Theory and Phenomenology in Particle Physics, Ed. A.Zichichi, Academic Press, N.Y. 1969.
9. S.B.Gerasimov, JETP 50, 1559 (1966).
10. N.Isgur, Phys.Rev.Lett., 36, 1262 (1976).
11. J.Schwinger. Phys.Rev. 135, B 816 (1964).
12. V.I.Ogievetsky. These proceedings.
13. B.J.Edwards, A.N.Kamal, Phys.Rev.Lett., 36, 241 (1976). Papers No 701 and 948.
14. P.J.O'Donnell. Phys.Rev.Lett., 36, 177 (1976). Paper No 882.
15. D.H.Boal et al. Phys.Rev.Lett., 36, 714 (1976), see also E.A.Ivanov, JINR E2-9430 (1975).
16. G.J.Gounaris. Paper No 981.
17. N.N.Achasov et al. ZhETP Pis'ma, 21, 497 (1975).
18. G.Parrour et al. Preprint LAL 1280, Orsay (1975).

THE NUCLEON AXIAL VECTOR FORM FACTOR FROM THRESHOLD π^+-ELECTROPRODUCTION

P.R.Norton

Daresbury Laboratory, United Kingdom

In this talk I shall review two papers.

307 A.Del Guerra, A.Giazotto, M.A.Giorgi, A.Stefanini, Pisa; D.R.Bottterill, H.E.Montgomery, P.R.Norton, Daresbury; G.Matone, Frascati.

504 A.S.Esaulov, A.S.Omelaenko, A.M.Pilipenko, Yu.I.Titov, Kharkov Inst.

1. G_A AND THRESHOLD π^+ ELECTROPRODUCTION

For massless pions one may use PCAC and current algebra to derive the transverse and scalar multipoles for π^+ electroproduction at threshold /1/.

For real pions a method is needed to extrapolate the unphysical $m_\pi = 0$ results to the physical pion mass. Specific models using different techniques have been used to derive the axial vector form factor from the measured cross sections /2-4/. Since there are small differences in detail between these models, we shall for consistency use that of Benfatto, Nicolo and Rossi to deduce G_A.

2. DATA OF DARESBURY-PISA-FRASCATI (#307)

The experiment was performed at momentum transfers of 0.45, 0.58 and 0.88 $(GeV/c)^2$. The electron was detected in a small-aperture focusing spectrometer and, in coincidence. The neutron in a 2x2 m^2 array of 145 blocks of plastic scintillator. Neutrons and protons were identified by additional thin scintillators in front of the array. A further counter telescope identified protons from radiative elastic scattering.

The cross section, measured up to W=1.13 GeV, was written as

$$\frac{1}{\Gamma_t} \, 4\pi \, \frac{K_L}{q^*} \, \frac{d^3\sigma}{dE' d\Omega_e d\Omega_\pi} = A_1 + Bq^{*2} + Cq^{*4} ,$$

where q^* is the π^+ c.m. momentum. The threshold cross section slope is

$$A_1 \sim |E_{0+}|^2 + \epsilon |k^2| |S_{0+}|^2 .$$

In this experiment the virtual photon polarization ϵ was ~ 0.94 and E_0^+ and S_0^+ could not be separated.

The results for A_1, together with some previous experimental measurements[5,6], are shown in Fig.1. The solid line is the prediction of the Devenish-Lyth fixed-t dispersion relation model[8], which is in excellent agreement with the data.

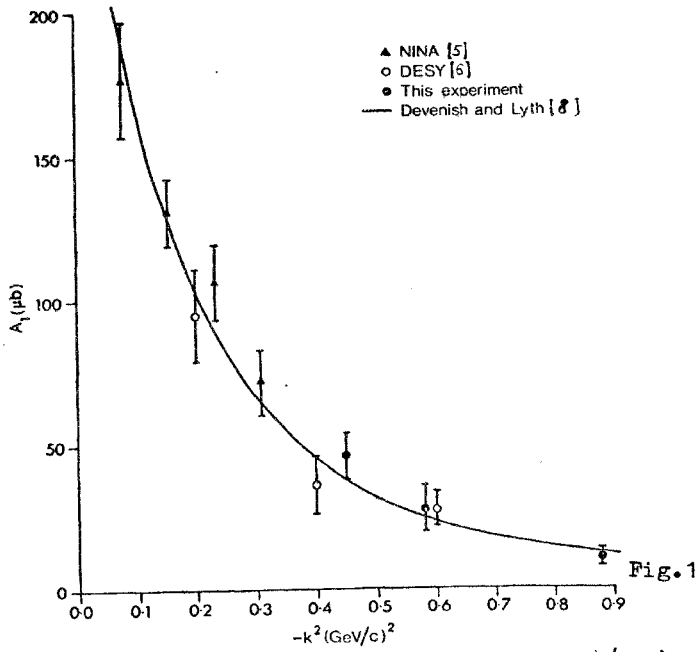

Fig.1

In Fig.2 are shown the values of $G_A(k^2)/G_A(0)$ deduced using the model of Benfatto, Nicolo and Rossi[2]. Assuming the dipole expression $G_A(k^2)/G_A(0) = \left(1 + \frac{|k^2|}{M_A^2}\right)^{-2}$ the best fit to all the data shown is $M_A = 0.96 \pm 0.03$ GeV. The dipole fit is preferred over the monopole. Using the parametrisation $G_A(k^2)/G_A(0) = 1/\left(1 + 2C_A|k^2| + C_B^2|k^2|^2\right)$ which is the monopole for $C_B = 0$, the dipole for $C_A = C_B$ we find the χ^2 contours shown in Fig.3. The dipole hypothesis is an excellent fit, but the data is within 2σ of the monopole.

This result, $M_A = 0.96 \pm 0.03$ GeV, is in excellent agreement with quasi-elastic neutrino scattering[9] which gives $M_A = 0.84 \pm 0.11$ GeV from the differential cross section and $M_A = 0.98 \pm 0.13$ GeV from the total cross section.

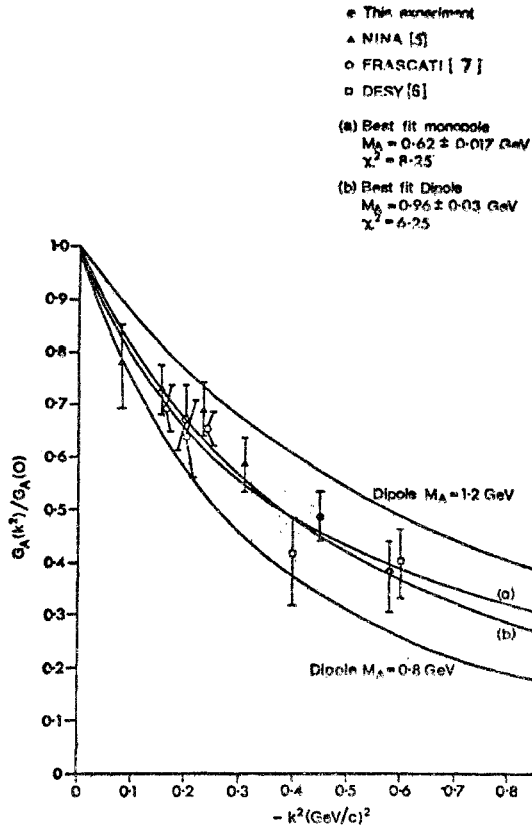

Fig.2

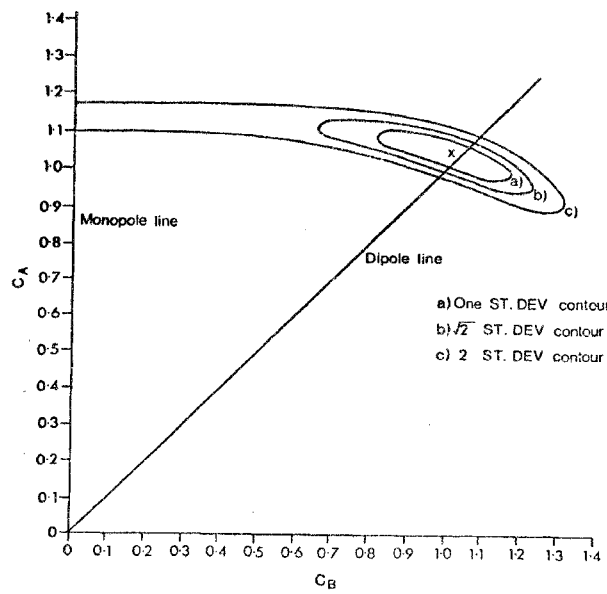

Fig.3

3. Data from Kharkov Inst. (# 504)

New data have been presented by the Kharkov Institute on a single-arm experiment at $|k^2| = 3.5$, 5.0 and 8.0 F^{-2}, in which the longitudinal and transverse contributions to the threshold cross section slope were separated by varying ϵ. Fig.4 shows the slope $\sum_t$, the sum of π^+ and π^0, defined by

$$\lim_{q^* \to 0} \left(\frac{1}{\Gamma_t} \frac{K_L}{q^*} \frac{M}{4\pi W} \frac{d^2\sigma}{dE' d\Omega_e} \right) = |E_{0+}|^2 + \epsilon |k^2| |S_{0+}|^2$$

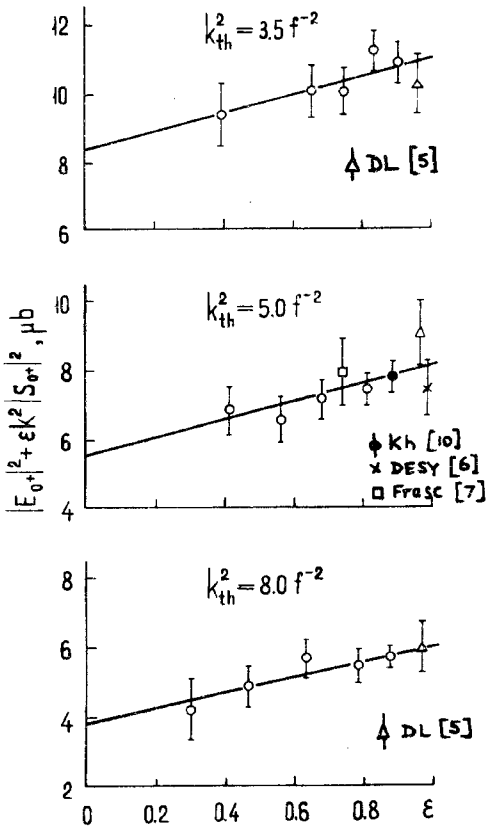

Fig.4

as a function of ϵ . The data are in agreement with previous measurements[5-7,10] (to which have been added a computed[2] π^0 contribution). The separated cross sections are shown in fig.5. The solid curve represents the BNR model with M_A=1 GeV, the dash-dot line the π^0 contribution (calculated) and the dashed line the PVBA without dispersion corrections[4].

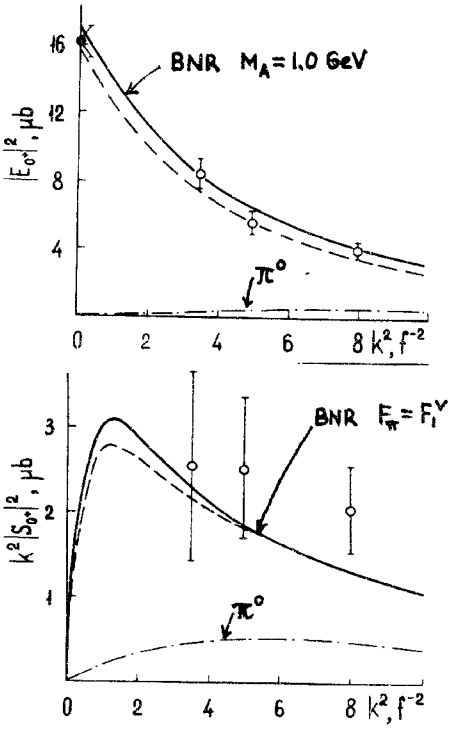

Fig.5

The values of $G_{TA}(k^2)/G_{TA}(0)$ deduced from the transverse cross section using the BNR model (0.78±0.03, 0.66±0.03, 0.57±0.03) are in excellent agreement with previous coincidence data. The pion form factor F_π deduced from $|S_{0+}|^2$ is consistent with previous determinations.

References

1. See ref.[5] for an extensive bibliography.
2. G.Benfatto, F.Nicolo and G.C.Rossi. Nucl.Phys., B50 (1972), 205, Nuovo Cimento 14A(1973)425.
3. G.Furlan et al. Nuovo Cimento 62A (1969)519.
4. N.Dombey and B.J.Read. Nucl.Phys., B60 (1973) 65.
   Yu.V.Kulish. Yader. Fiz. 13 (1971)1301.
5. A. Del Guerra et al. Nucl.Phys., B99 (1975) 253.
6. P.Brauel et al. Phys.Lett., 45B (1973)389; 50B (1974) 407.
7. E.Amaldi et al. Phys.Lett., 41B (1972) 216.
8. R.C.E.Devenish and D.H.Lyth. Nucl.Phys., B93 (1975) 109.
9. S.J.Barish et al. Talk by D.H.Perkins, Stanford Conf. 1975.
10. Yu.I.Titov et al. Pisma v. ZHETF 12 (1970)186.

SHADOWING EFFECT IN INELASTIC ELECTRON SCATTERING ON ^{12}C AND ^{27}Al NUCLEI AT SMALL FOUR MOMENTUM TRANSFER

S.Hartwig, F.H.Heimlich, G.Huber, E.Rössle, J.Bleckwenn, M.Köbberling, J.Moritz, K.H.Schmidt, D.Wegener, D.Zeller, P.David, H.Mommsen

DESY, FRG

The inelastic electron scattering on nucleons and nuclei can be described as an absorption process of virtual photons by hadronic matter, characterized by the absorption cross section

$$\sigma = \sigma_t + \varepsilon \sigma_l = \frac{1}{\Gamma_t} \frac{d^2\sigma}{d\Omega dE}$$

Γ_t is the flux of virtual photons, $\frac{d^2\sigma}{d\Omega dE}$ is the measured twofold electron scattering cross section[1]. For real high energetic photons it was shown that the number of effective nucleons A_{eff} of a nucleus is smaller than its atomic number A[2]. This effect, well known for absorption processes where hadrons are involved[3], has been explained by the vector meson dominance model to be due to a hadronic component of the photon[4,5]. On the other side it is known from deep inelastic electron scattering that at four momentum transfers $q^2 \gtrsim 1$ (GeV/c)^2 the interaction between the virtual photon and the hadron has a point-like structure. Therefore it is of interest to study the damping of the photons hadronic component by increasing the mass q^2 of the virtual photon[5]. Foregoing experiments have found weak evidence for shadowing effects, which influence the absorption of virtual photons on nuclei[6]. In order to study this effect in more detail we have measured the inelastic electron scattering cross section on hydrogen, deuterium, ^{12}C and ^{27}Al nuclei for 0.075(GeV/c)^2 $\leq q^2 \leq$ 1 (GeV/c)^2 and energies of the virtual photon $\nu <$ 6.2 GeV at the DESY synchrotron[7].

The scattered electrons have been detected by a spectrometer consisting of a bending magnet, four wire spark chambers, trigger and particle identifying counters[7,8]. The typical statistical error of the data is 2% to 4% and the systematical error of the data is 3.5%.

The main corrections, which had to be applied to the raw data, were due to radiative processes. The calculations have been performed using the formulae of Mo and Tsai[9] for the radiative tail of the elastic electron scattering and the formula of Tsai[10] for the elastic electron scattering. We have used the formfactors of Hofstadter[11] to determine the radiative tail of elastic electron scattering on ^{12}C and ^{27}Al. If necessary the parametrization of the nucleus formfactor has been extrapolated to regions of the data four momentum transfer where no experimental data were available.

The influence of different sources of the radiative corrections has been studied by comparing the measured absorption cross section $\sigma_{\gamma A}$ on a nucleus with the corresponding one on nucleons:

$$\tau = \frac{A_{eff}}{A} = \frac{\sigma_{\gamma A}}{A(1-\frac{N}{\omega})\sigma_{\gamma P}}$$

$\sigma_{\gamma P}$ absorption cross section for virtual photons on protons,

$$\omega = \frac{2M\nu + M^2}{q^2}$$

M = nucleon mass, N number of neutrons. If the radiative process is not modified by the fact, that in a nucleus part of the possible final states, accessible to the scattered nucleon, are occupied by spectator nucleons, the radiative tail due to the contribution of (quasi-) elastic electron nucleon scattering should factorize in the measured inelastic electron nucleus scattering and this contribution to radiative corrections should cancel in the ratio $\tau = A_{eff}/A$. Under this assumption the only corrections which have to be taken into account are due to the radiative tail from elastic electron-nucleus scattering. In Fig. 1a typical results of the present experiment are plotted for the case that the factorization assumption holds. The data show clear evidence for a shadowing effect at small four momentum transfers

At small q^2, where the momentum of the struck nucleon after the scattering process is small, the occupation of possible final states by spectator nucleons will be of influence. Because of the Pauli principle the contribution of the

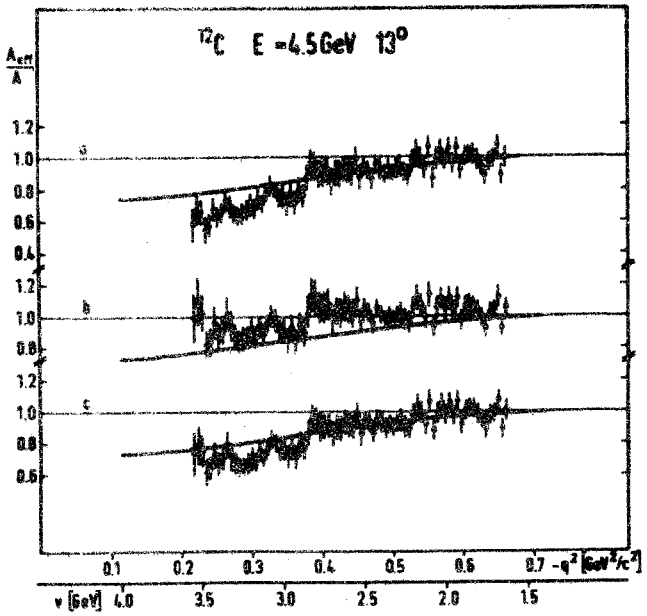

Fig. 1. Ratio A_{eff}/A for ^{12}C Primary electron energy E_e =4.5GeV, electron scattering θ_e = 13°. The figures a,b,c are for different treatments of the radiative corrections (see text).

quasi-elastic radiative tail should decrease compared to the radiative tail of elastic electron nucleon scattering. In the extreme the radiative tail contributes to the measured cross section only for free electron-nucleon scattering, while the electron doesn't radiate for electron-bound state nucleon scattering, because all possible final states are occupied. This extreme case is handled, if one applies only radiative corrections due to elastic electron proton scattering, but no corrections due to electron-bound state nucleon scattering. The result of this procedure is shown in fig . 1b, The shadowing effect nearly disappears. A realistic correction should yield results for the ratio $r = A_{eff}/A$ between the two extreme cases of fig. 1a and fig . 1b respectively.

An approach to the realistic computation of radiative corrections due to the radiative tail of electron-bound state nucleon scattering was given by Bernabeu[12]. He has described the influence of the Pauli principle to the quasi-elastic electron nucleon scattering by an effective nucleon formfactor. We have used this effective formfactor to compute the radiative correction of quasi-elastic scattered electrons. The results of this analysis are given in fig. 1c, showing clear evidence for a shadowing effect on both nuclei.

In fig. 2 the ratio $r = A_{eff}/A$ for ^{27}Al is plotted as a function of the scaling variable $x = q^2/(2M\nu)$ together with data of Stein et al.[6]. In both cases radiative corrections, using the method of fig. 1c have been applied. The general agreement between the two data sets is quite satisfying. The sharp increase of the shadowing at low values of q^2 in our data is due to the neglection of the Pauli principle effect discussed above. The full curve in fig. 2 is the prediction of the generalized vector dominance model[5] for ^{207}Pb

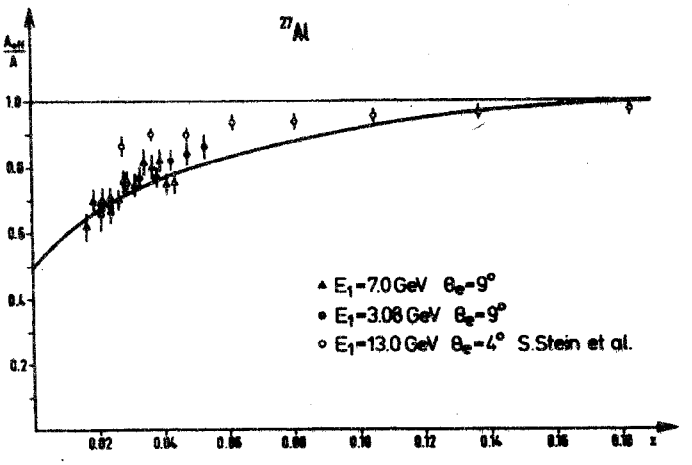

Fig. 2. Ratio A_{eff}/A for ^{27}Al as a function of the scaling variable x. The full curve is the theoretical prediction of the generalized vector meson dominance model for ^{207}Pb [5].

In conclusion we have shown that a shadowing effect exists for the absorption cross section of virtual photons. It increases with decreasing values of the scaling variable x. For comparison with theoretical predictions one has to take into account the differences of the radiative tails of electron scattering on free and bound state nucleons respectively.

Theoretical prediction of improved version of the generalized vector dominance model[13] are in agreement with the data of the present experiment.

We acknowledge the untiring help of H.Sindt during all stages of the experiment. this work has been supported by the Bundesministerium für Forschung und Technologie.

REFERENCES

1. L.Hand. Phys.Rev., 129, 1834 (1963).
2. V.Heyne, H.Meyer, B.Naroska, D.Notz. Phys.Lett., 34B, 651 (1971).
3. G. Belletini et al. Nucl.Phys., 79, 609 (1966).
4. S.Brodsky, J.Pumplin. Phys.Rev., 182, 1794 (1969).
5. D.Schildknecht. Nucl.Phys., B66, 398 (1973).
6. S.Stein, W.B.Atwood, E.D.Bloom, R.L.A.Cottrell, H. De Staebler, C.L.Jordan, H.G.Piel, C.Y.Prescott, R.Siemarn, R.E.Taylor. Phys.Rev., D12, 1884 (1975). W.R.Ditzler et al. Phys.Lett., 57B, 201 (1975).
7. G.Huber. Thesis, Friberg University, 1976 and DESY Internal Report F23/76-1.
8. S.Galster, G.Hartwig, H.Klein, J.Moritz, K.H.Schmidt, W.Schmidt-Parzefall, D.Wegener, J.Bleckwenn. Phys.Rev., D5, 519 (1972).
9. L.W.Mo, Y.S.Tsai. Rev.Mod.Phys., 41, 205 (1969).
10. Y.S.Tsai. Phys.Rev., 122, 1898 (1961).
11. R.Hofstadter. Ann. Rev.Nucl.Sci., 7, 231 (1957).
12. J.Bernabeu. Nucl.Phys., 186 (1972).
13. Paper No. 487, 490, 491.

SMALL-ANGLE COMPTON SCATTERING ON HYDROGEN AND DEUTERIUM

L.Criegee, G.Franke, A.Ciese, Th.Kahl, G.Poelz, U.Timm, H.Werner, W.Zimmermann

(Presented by D.Wegener, University of Karlsruhe)

We have measured Compton scattering on hydrogen at 6 GeV, and in a second, slightly modified experiment on hydrogen and deuterium at 5 GeV, both at particularly small momentum transfers ranging from -0.004 to -0.08 $(GeV/c)^2$ at 6 GeV and from -0.002 to -0.06 $(GeV/c)^2$ at 5 GeV.

The experimental set up and the analysis procedure is described in paper No. 1016 on this conference.

The differential cross sections determined in this way are shown in Fig. 1. Only statistical errors are shown. Systematic errors result mainly from the uncertainty of the background $\pi^0+\eta$ ($\pm$1%) of the converter position ($\pm$1.5%), and in the case of the 6 GeV data from the error in the telescope efficiencies ($\pm$1.5%). By quadratic addition to the normalization error we obtain a total systematic error of $\pm$2.5% at 5 GeV and $\pm$3.6% at 6 GeV.

Fig. 2. shows the data of this experiment together with those of other DESY and SLAC experiments[1,2].

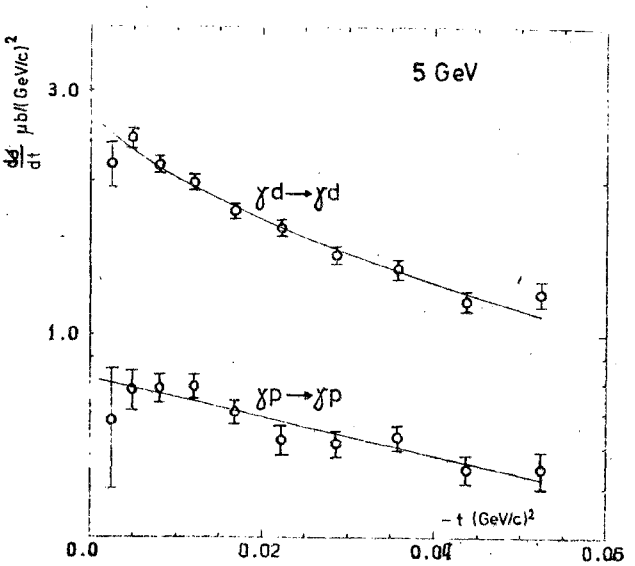

Fig. 1. Compton scattering on hydrogen and deuterium.

A fit to our data of the form $\frac{d\sigma}{dt} = A \exp(Bt)$ as suggested by diffraction theory, yields the results shown in Table 1. The errors include statistical errors as well as the total systematic error.

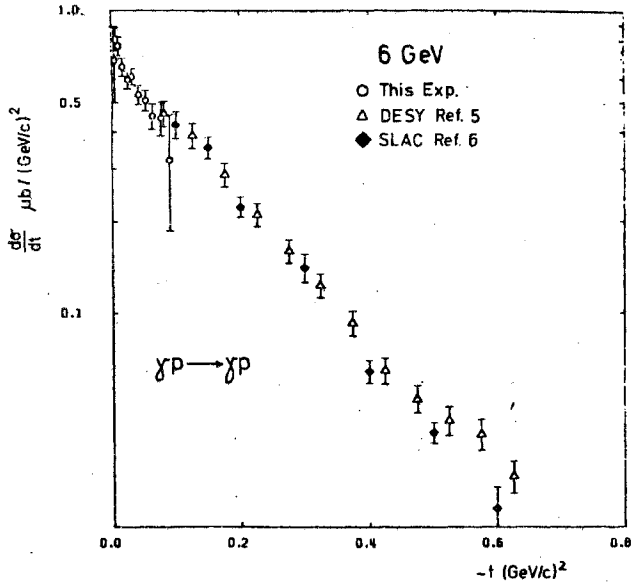

Fig. 2. Differential Compton cross section on hydrogen.

Table 1

	Photon energy GeV	$(GeV/c)^2$	$(GeV/c)^{-2}$
This experiment	5	0.82±0.04	8.5±1.5
	6	0.79±0.04	8.6±1.2
DESY/5/	4–6.2	0.84±0.08	5.7±0.35
SLAC/7/	8	0.82±0.04	7.7±0.5
VDM Prediction (see text)	5	0.46±0.05	-
	6	0.44±0.04	-

The extrapolated forward cross sections are shown as a function of energy in Fig. 3 together with those from other experiments/1-3/. The curve shows the contribution of the spin-independent amplitude f_1 in the standard decomposition

$$\frac{d\sigma}{dt}(0) = \frac{\pi}{k^2}\left(|f_1|^2 + |f_2|^2\right),$$

where f_2 is the spin-dependent amplitude, and k the photon energy, f_1 was calculated from the total cross section via optical theorem and dispersion relation/4/. Our extrapolated forward cross sections are 10% smaller than the predictions, but consistent within the errors. They are compatible with a vanishing spin dependent amplitude f_2 at both energies.

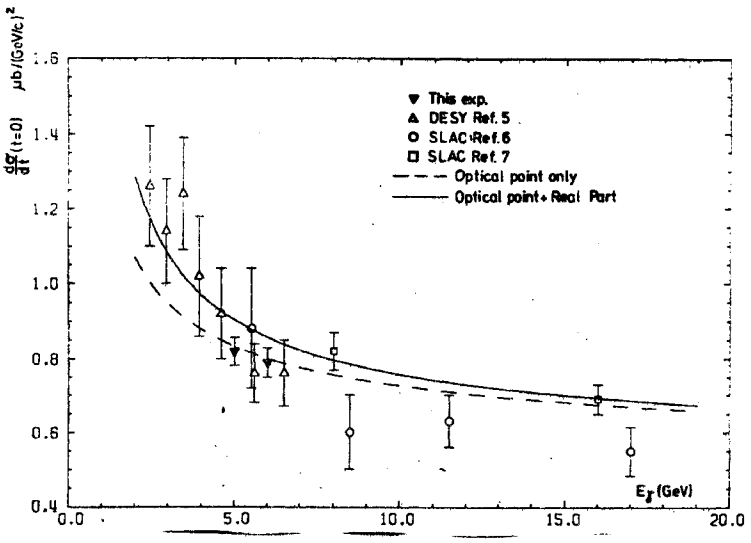

Fig. 3. Differential forward Compton cross section on hydrogen.

For comparison with the predictions of the vector dominance model, VDM, the forward cross sections have been calculated using the sum rule

$$\frac{d\sigma}{dt}(\gamma p \to \gamma p) = \left[\sum_V \frac{\alpha}{4}\frac{4\pi}{\gamma_V^2}\left(\frac{d\sigma}{dt}(\gamma p \to V p)\right)^{1/2}\right]^2$$

with recent values for the vector meson cross sections/5/ and the Orsay values for the coupling constants $\frac{\alpha}{4}\frac{4\pi}{\gamma_V^2}$ /6/. Table 1 demonstrates the well known discrepancy: The data are higher by about 40% than the VDM predictions. This discrepancy can be removed by including the higher vector mesons $\varphi'(1600)$, $\psi(3100)$ and $\psi(3700)$ and by extending the VDM to the GVDM/7/.

The differential cross section for the deuteron (Fig. 1) shows the transition from coherent scattering at low $|t|$ to incoherent scattering at higher $|t|$ values. Neglecting spin effects the cross section can be written in closure approximation as

$$\left(\frac{d\sigma}{dt}\right)_d = \frac{2\pi}{k^2}\left[|a_0|^2(1+F(t)) + |a_1|^2(1-F(t))\right] G(t)$$

where is the proton energy. $F(t)$ and $G(t)$ denote the deuteron form factor and the Glauber correction factor/8/. a_0 and a_1 are the amplitudes of isospin 0 and 1 exchange. The influence of the Fermi motion/9/ is smaller than the Glauber correction, according to our own calculations/10/. The corresponding differential proton cross section is given by

$$\left(\frac{d\sigma}{dt}\right)_p = \frac{\pi}{k^2}\left(|a_0|^2 + |a_1|^2 + 2\,\mathrm{Re}\,(a_0 a_1^*)\right)$$

From the deuteron and the proton cross sections

one can deduce the two isospin ratios $|a_1|^2/|a_0+a_1|^2$ and $Re(a_0 a_1^*)/|a_0+a_1|^2$. By a fit to our experimental data we obtain the values listed in Table 2. Systematic errors resulting mainly from the uncertainty in the $\pi^0\eta$ background component and in the precise converter position, amount to about half of the statistical errors, while normalization errors common to both targets should have no effect.

The isospin ratios depend however sensitively on the assumed shape of $F(t)$ and $G(t)$. We have used a deuteron wave function following Reid and calculated $G(t)$ in the ϱ-dominance approximation. If we analyse the data starting from a Hulthen wave function[12], we obtain consistent, although numerically different ratios. For comparison we have also calculated these parameters from the data[3] using our Glauber corrections. The values are then changed slightly in Table 2.

Table 2

Ratios of isospin amplitudes with statistical errors. *Calculation with Hulthen wave function. ** Analysis of the data from Ref.[3]) using a deuteron wave function by Reid[10,11]

	$\frac{\lvert a_1\rvert^2}{\lvert a_0+a_1\rvert^2}$	$\frac{Re(a_0 a_1^*)}{\lvert a_0+a_1\rvert^2}$
This experiment, 5 GeV	0.13±0.09 (0.08±0.10	0. ±0.03 0.02±0.03)*
SLAC[7] 8 and 16 GeV	0.03±0.10 (0.04±0.11)	-0.049±0.012 (0.007±0.018)**
DESY[17]	$\frac{Im\,a_1}{Im\,a_0}$ = 0.042±0.008	

All the ratios are compatible with a vanishing or at least small isospin 1 exchange contribution to photon nucleon interaction. They are also compatible with the measured[13] ratio

$$\frac{Im\,a_1}{Im\,a_0} = \frac{\sigma(\gamma p)-\sigma(\gamma n)}{\sigma(\gamma p)+\sigma(\gamma n)}$$

as listed in Table 2, if one assumes equal real to imaginary part of the a_1 amplitude as predicted for A_2 Regge exchange.

We are indebted to the technicians and to the members of the Hallendienst who made the experiment possible. We are grateful to the scientific directors of DESY for their interest into our experiment.

REFERENCES

1. G.Buschhorn et al. Phys.Lett., 37B, 207 (1971).
2. R.L.Anderson et al. Phys.Rev.Lett., 25, 1218 (1970).
3. A.M.Boyarski et al. Phys.Rev.Lett., 26, 1600 (1971); 30, 1098 (1973).
4. M.Damashek, F.J.Gilman. Phys.Rev., 1D, 1319 (1970).
5. J.Ballam et al. Phys.Rev., 7D, 3150 (1973).
6. J.Perez-Y-Jorba. In Proc. 4th Int. Symp. on El and Phot. Int. at High En., Liverpool (1970).
7. J.J.Sakurai, D.Schildknecht. Phys.Lett., 42B, 216 (1972) and literature cited there.
8. V.Franco, R.J.Glauber. Phys.Rev., 142, 1195 (1966).
9. W.B.Atwood and G.B.West. Phys.Rev., D7, 773 (1973).
   A.Bodek. Phys.Rev., D8, 2331 (1973).
10. G.Poelz. Private communication.
11. R.V.Reid. Ann.Phys., 50, 411 (1968).
12. G.F.Chew, H.W.Lewis. Phys.Rev., 84, 779 (1951).
13. See e.g., G.Wolf. In Proc. 5th Int.Symp. on El and Phot. Int. at High En., Cornell University, 1971.

DETECTION OF $\pi\mu$ COULOMB BOUND STATES

R.Coombes, R.Flexer, A.Hall, R.Kennelly,
J.Kirkby, R.Piccioni, D.Porat, M.Schwartz,
R.Spitzer, J.Toraskar, S.Wiesner
Stanford University, Stanford, California
B.Budick, J.W.Kast
New York University, New York, N.Y.

We report herewith the detection of hydrogen-like atoms consisting of a negative (or positive) pion and a positive (or negative) muon in a Coulomb bound state. These $\pi\mu$ atoms are formed when the π and μ from the decay have sufficiently small relative momentum to bind. We have observed these atoms, produced at relativistic velocities, in the course of an experimental program at the Brookhaven A.G.S.

The basic properties of these atoms are calculated by the formalism used to describe the hydrogen atom. The reduced mass of the system is 60.2 MeV/c^2, its Bohr radius is 4.5×10^{-11}cm and the binding energy of the 1S state is 1.6 keV. To our knowledge, the first calculation of the branching ratio $R = \frac{K_L \to (\pi\mu)_{Atom} + \nu}{K_L \to ALL}$ was carried out by Nemenov[1], who found that $R \sim 10^{-7}$, with the precise value depending upon the form factors of K_L^0 decay. We will present our results on R in a subsequent paper; only the evidence related to the detection of these atoms is discussed herein.

The prime motivations for the experiment are twofold. First, the value R is proportional to the square of the $\pi\mu$ wave function at very small distances and so an anomaly in its value may be indicative of an anomaly in the $\pi\mu$ interaction. Secondly, by passing the atoms through a magnetic field at high velocity the 2s states should be depopulated through stark mixing with the 2P states and consequent decay to the 1S states. The extent of this depopulation will be highly dependent upon the vacuum polarization shift (Lamb shift) of the 2P states relative to the 2S states and may, if measured with some accuracy lead to a determination of the pion charge radius.

The K_L^0 particles which give rise to our "atomic beam" are produced by a 30 GeV proton beam striking a 10 cm beryllium target (see Figure 1). A large vacuum tank and a connecting evacuated beam channel lead out to the detection equipment. A 4 ft steel collimator prevents any direct line of sight from the detector system to the target.This is to prevent background particles, in particular K_L^0's from approaching the neighborhood of our detectors.

Those K_L^0's which decay within the shaded area in the vacuum tank give rise to decay products which may, if properly oriented in their direction of motion, travel down the channel. In order to remove charged particles, we have interposed two magnets along this channel. The first of these, labeled the "sweeping magnet" bends horizontally and has an integrated field strength of 8 kilogauss meters. The second magnet, (originally intended to induce transitions between the 2s and 1s states of these atoms) is called the "transition magnet" and bends vertically with an integrated field strength of 36 kilogauss-meters. Those charged particles which survive have very high momenta or are given a significant deflection before entering the detector region.

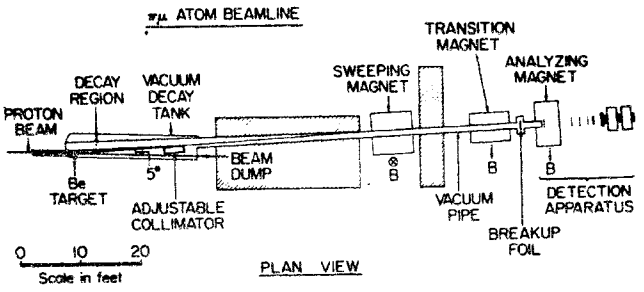

Fig. 1. Experimental arrangement at the A.G.S.

We have then a beam consisting largely of γ rays (resulting from π^0's which are in turn the products of kaon decays), highly energetic pions and muons, and occasional atoms. The momentum spectrum of the atoms coming down the channel has no appreciable contribution about 5 GeV/c.

To dissociate the atoms and make their detection possible, we interpose a thin aluminium foil before the end of the vacuum channel (see Fig. 2). Ionization of an atom takes place through a series of sequential transitions through the states having highest angular momentum for any given principal quantum number. We have calculated the thickness of foil required to break up a π-μ atom to be 0.025 cm of aluminium. In the course of the experiment, data was taken with foil thickness of 0.075 cm and 0.625 cm of aliminium.

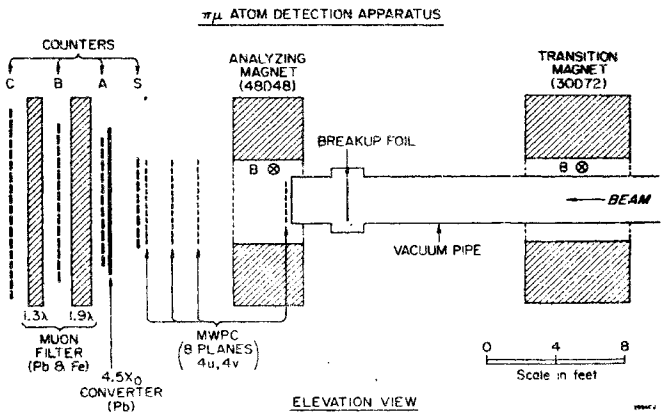

Fig. 2. Detection Apparatus.

The pion and the muon, now uncoupled, exit the foil at the same velocity (with momenta in the ratio of their rest masses) and in almost perfect spatial coincidence. The opening angle between them at a typical atomic momentum of 3 GeV/c, neglecting the multiple scattering in the foil, should be less than 0.5 milliradians. The projected multiple scattering of each particle in a 0.030'' aluminium foil is about (1.3/p (GeV)) milliradians. Thus the angle between pion and muon upon emerging from a 0.075 cm foil should be about two milliradians. The angle between them in the case of a 0.625 cm aluminium foil is about 5 miliradians.

We next introduce these two coincident particles into a horizontal field which serves to separate them vertically. We terminate the vacuum channel with a thin mylar window where the separation between the pion and muon is about a centimeter for a typical atom. Just beyond the window we place a multiwire proportional chamber made of two planes (planes 1 and 2) to allow the reconstruction of the vertical and horizontal coordinate or each of the particles. Each of these planes is constructed of a set of wires inclined at 60° to the vertical. At the point where the pion and the muon traverse these planes they are directly above one another and separated by a vertical distance Δ which is closely correlated to the sum of their momenta.

After leaving the analyzing magnet the pion and the muon continue through a series of three further pairs of proportional chambers, each constructed of wires at $\pm 60^\circ$ to the vertical. In each of these planes the x and y coordinates of each track can be localized to about $\pm$ 1 mm. Following the last of these chambers, we have, in sequence: a bank of 11 counters (S bank), a sheet of 1'' thick lead to induce showering of electrons, a bank of 15 counters (A bank), a lead and steel wall embodying 1.9 mean free paths of absorber, another bank of 19 counters (B bank), a wall comprising 1.3 free paths of absorber and a final bank of 23 counters (C bank). The absorber removes muons below a momentum of 0.9 GeV/c and about 90% of the pions. The first crude indication that an event of interest has passed through the detector comes when we obtain a trigger indicating simultaneous counts in two S counters, two non-adjacent A counters, one or more B counters and one or more C counters. We next examine planes 1 and 2 to determine rapidly whether two tracks passed directly above one another within the experimental reso-

lution and with Δ lying between .8 and 3.5 centimeters. We then remove, through the use of our on-line computer, all events in which more than four tracks passed through the first plane. The residual events are logged for further study. The information recorded includes the timing of all counters, the pulse height on each of the A counters and the positions of the tracks as they pass through the eight planes.

We carry forth the analysis of the data by subjecting each event to a sequence of tests, each of which must be passed before it can be considered a valid candidate for a π-μ atom. The geometrical characteristics of these tests have been determined through a study of the e^+-e^- pairs which are created by γ rays impinging on the foil and the muons which come down the vacuum channel when the sweeping and transition magnets are turned off. The tests are as follows:

1. All counters involved in a trigger must be time coincident within ± 2 nanoseconds after correction for flight times of the various particles.

2. The four counters which define the muon track must lie on a straight line within the limits of Coulomb scattering in the absorber. Only one track may penetrate to the C bank.

3. The pulse height on each of the counters must be less than 2.5 times that produced by a minimum ionizing particle.

4. Each of the tracks must have a momentum not less than 0.9 GeV/c.

5. After the two tracks are reconstructed back through the magnet, we can determine the X and y projections of their apparent separation and the apparent angle between them as they left the foil.

The cuts are as follows:

a) The vertical separation at the foil must be less than 1.35 cm.

b) The horizontal separation at the foil must be less than 0.50 cm.

c) The measured vertical angle between the two tracks as they leave the foil must be less than 0.025 radiane.

d) The measured horizontal angle between the two tracks as they leave the foil must be less than 0.004 radians.

6. Our study of the e^+e^- pairs indicates that the vertical spacing, Δ between the two tracks in planes 1 and 2 is predictable to a wire spacing given the momenta of the two particles. We reject all candidates which do not conform to this constraint within ± 2 wire spacings.

7. By studying the e^+e^- pairs we have ascertained that we can project our tracks back to the vicinity of the collimator with a horizontal spatial resolution of ± 2.5 cm. We insist then that all of our tracks of interest point back to 22.5 cm wide fidicial region near the collimator, missing both the collimator itself and the walls of the vacuum channel.

8. Finally, we insist that the sum of the pion and muon momenta be no more than 5 GeV/c.

Having subjected all of the recorded data to these tests, we arrive at a residue of 33 events. For each of these events we plot (in Fig. 3) the parameter $\alpha = \frac{P_\pi - P_\mu}{P_\pi + P_\mu}$ where P_π is the pion momentum and P_μ is the muon momentum. A study of this parameter through an examination of e^+e^- pairs indicates that the acceptance of our apparatus, modified by the abovementioned

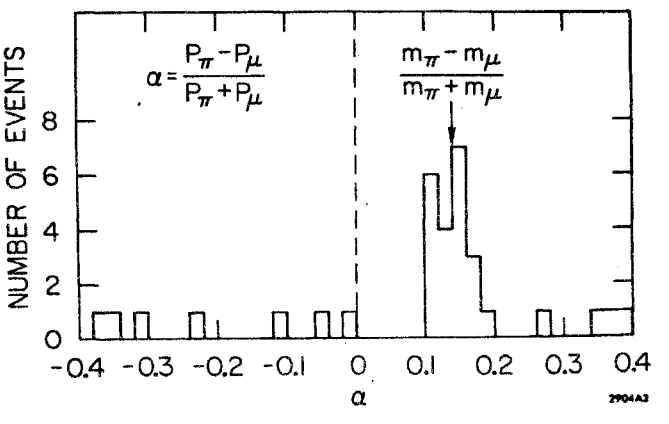

Fig. 3. A plot of the parameter α indicating the detection of π-μ atoms.

tests, is flat within 30% from α = -0.4) to α = +0.4. None of our acceptance tests bias us toward one or another sign of α. Hence, any bump in this plot would indicate a strong correlation between pion and muon momenta; in particular the atoms should be characterized by a value of $\alpha = \frac{m_\pi - m_\mu}{m_\pi + m_\mu} = 0.14$ The data shows a clear peak at the predicted point containing a total of 21 events with an estimated background of 3 events. The width of the peak is consistant with that expected from measurement errors.

We conclude that we have observed Coulomb bound states of pions and muons.

We would like to express our appreciation to the Brookhaven A.G.S. staff and to L.Birkwood, J.Bjorken, S.Drell, G.Donaldson, M.Faessler, M.K.Gaillard, D.Hitlin, B.Kincaid, D.Ouimette, M.Prasad, C.Rasmussen, A.M.Rushton, J.Tannis, A.Tilgham, J.D.Waleoka, S.Wojcicki and C.Zupancic for valuable assistance.

REFERENCES

1. L.L.Nemenov. Sov. Journ. of Nucl.Phys., 16, 67 (1973).